The evolution of rock friction is more sensitive to slip than elapsed time, even at near-zero slip rates

Pathikrit Bhattacharya[1], Allan M Rubin[2], Terry E Tullis[3], Nicholas M Beeler[4], and Keishi Okazaki[5]

[1]National Institute of Science Education and Research, Bhubaneswar
[2]Princeton University
[3]Brown University
[4]U.S. Geological Survey
[5]Kochi Institute for Core Sample Research

November 30, 2022

Abstract

Nearly all frictional interfaces strengthen as the logarithm of time when sliding at ultra-low speeds. Observations of also logarithmic-in-time growth of interfacial contact area under such conditions has led to constitutive models which assume that this frictional strengthening results from purely time-dependent, and slip-insensitive, contact area growth. The main laboratory support for such strengthening has traditionally been derived from increases in friction during 'load-point hold' experiments, wherein a sliding interface is allowed to gradually self-relax down to sub-nanometric slip rates. In contrast , following step decreases in the shear loading rate, friction is widely reported to increase over a characteristic slip scale, independent of the magnitude of the slip-rate decrease-a signature of slip-dependent strengthening. To investigate this apparent contradiction, we subjected granite samples to a series of step decreases in shear rate of up to 3.5 orders of magnitude, and load-point holds of up to 10,000 s, such that both protocols accessed the phenomenologi-cal regime traditionally inferred to demonstrate time-dependent fric-tional strengthening. When modeling the resultant data, which probe interfacial slip rates ranging from 3 μm/s to less than 10ˆ-5 μm/s, we found that constitutive models where low slip-rate friction evolution mimics log-time contact area growth require parameters that differ by orders of magnitude across the different experiments. In contrast, an alternative constitutive model in which friction evolves only with interfacial slip fits most of the data well with nearly identical parameters. This leads to the surprising conclusion that frictional strengthening is dominantly slip dependent even at sub-nanometric slip rates.

The evolution of rock friction is more sensitive to slip than elapsed time, even at near-zero slip rates.

Pathikrit Bhattacharya[a,b], **Allan M. Rubin**[b], **Terry E. Tullis**[c], **Nicholas M. Beeler**[d], **and Keishi Okazaki**[e]

[a]School of Earth and Planetary Sciences, National Institute of Science Education and Research, Bhubaneswar, India; [b]Department of Geosciences, Princeton University, Princeton, NJ, United States.; [c]Department of Earth, Environmental and Planetary Sciences, Brown University, Providence, RI, United States; [d]U.S. Geological Survey, Vancouver, WA, United States; [e]Kochi Institute for Core Sample Research, Japan Agency for Marine-Earth Science and Technology (X-star, JAMSTEC), Kochi, Japan

This manuscript was compiled on August 8, 2021

Nearly all frictional interfaces strengthen as the logarithm of time when sliding at ultra-low speeds. Observations of also logarithmic-in-time growth of interfacial contact area under such conditions has led to constitutive models which assume that this frictional strengthening results from purely time-dependent, and slip-insensitive, contact area growth. The main laboratory support for such strengthening has traditionally been derived from increases in friction during 'load-point hold' experiments, wherein a sliding interface is allowed to gradually self-relax down to sub-nanometric slip rates. In contrast, following step decreases in the shear loading rate, friction is widely reported to increase over a characteristic slip scale, independent of the magnitude of the slip-rate decrease – a signature of slip-dependent strengthening. To investigate this apparent contradiction, we subjected granite samples to a series of step decreases in shear rate of up to 3.5 orders of magnitude, and load-point holds of up to 10,000 s, such that both protocols accessed the phenomenological regime traditionally inferred to demonstrate time-dependent frictional strengthening. When modeling the resultant data, which probe interfacial slip rates ranging from 3 μms^{-1} to less than $10^{-5}\mu ms^{-1}$, we found that constitutive models where low slip-rate friction evolution mimics log-time contact area growth require parameters that differ by orders of magnitude across the different experiments. In contrast, an alternative constitutive model in which friction evolves only with interfacial slip fits most of the data well with nearly identical parameters. This leads to the surprising conclusion that frictional strengthening is dominantly slip dependent even at sub-nanometric slip rates.

Fault friction | Earthquake | Tribology

Frictional surfaces across a wide range of materials are known to strengthen at low sliding rates. In the laboratory, this strengthening is often explored through slide-hold-reslide experiments, where a sample previously driven at a constant sliding speed is perturbed by abruptly holding the external load at fixed displacement or a fixed, low, stress level (1–8). In the former protocol, which we call a load-point hold, slip along the frictional interface continues at an ever-decreasing rate as the mechanical system (testing machine plus sample) elastically unloads and the shear stress on the frictional interface decreases. For hold durations longer than a few seconds, the static friction peak observed upon resliding at the pre-hold rate has been shown to increase as the logarithm of the hold duration, across a wide range of materials including rocks (1, 4, 5, 8, 9) (Figure S1).

In providing a physical explanation for these observations of frictional strengthening, reference has often been made to the similarly logarithmic-in-time growth of interfacial contact area (in transparent polymer glasses and plastics) during periods of little to no slip (10, 11). The connection of frictional strength to contact area dates back to Bowden and Tabor (12), who imagined frictional strength of an interface (τ_f) as the product of an average velocity dependent contact strength (τ_c) (6) and the ratio of the real contact area to the total contact area (Σ_r): $\tau_f = \tau_c\Sigma_r$. Logarithmic growth of contact area is expected if contacts deform via thermally-activated creep at normal stresses close to the indentation hardness of the sample (6, 8, 13). In the Bowden and Tabor view, this contact area growth then leads to a logarithmic-in-time increase in friction measured relative to the steady-state pre- and post-hold sliding rate. One consequence of this view is that the strength increase during the hold portion of slide-hold-reslides should be predictable from the hold duration alone, and be insensitive to the small amount of interfacial slip that accumulates during the hold (4).

The largely empirical rate-state friction (RSF) equations are widely used to model such time-varying friction phenomenology in rock (4, 5, 14) and a diverse set of industrial materials (6, 15–19). However, the two most widely used versions offer opposing views of the importance of slip for friction evolution. The more commonly used Aging formulation (1, 14) predicts that frictional strengthening loses all sensitivity to slip whenever the

Significance Statement

For many decades, frictional strength increase at low slip rates has been ascribed to time-dependent contact area growth across the sliding interface. As a result, phenomenological models that correctly predict contact area growth as observed in laboratory experiments have also been widely assumed to be appropriate descriptors of frictional strength evolution. We present new experiments which impose more than 5 orders-of-magnitude slip rate reductions on granite to show that frictional strength evolution in these rocks unequivocally refutes such models. Instead, the data suggests that, even at sub-nanometric slip rates, frictional strength dominantly evolves with accrued slip. This remarkable slip-sensitivity of friction requires changes of intrinsic strength of the interface with slip that are absent from popular conceptual models of friction at the microscopic contact-scale.

P.B. and A.R. conceived the experiments; T.T. and K.O. performed the experiments; P.B. analyzed the data and wrote the manuscript; all authors provided inputs on the manuscript.

All authors declare no conflict of interest.

[2]To whom correspondence should be addressed. E-mail: path_geoalum alumni.princeton.edu

interface is subjected to a sufficiently large and rapid decrease in slip rate. In the limit of a truly stationary interface, it implies strengthening as the logarithm of time, even in the absence of slip. When viewed in conjunction with the evidence for log-time growth of contact-area across stationary interfaces, this is consistent with the Bowden and Tabor view of contact area being the primary determinant of macroscopic strength. Its more empirical alternative – the Slip formulation – instead predicts no strengthening in the absence of sliding, and retains slip-sensitivity at all slip rates (20).

Over the last three decades, phenomenological details of frictional strengthening derived from laboratory slide-hold-reslide experiments have been widely interpreted as supporting the Aging formulation view – that frictional strengthening loses sensitivity to slip under the extreme slip-rate reductions imposed during load-point holds (3–7, 21). In contrast, friction evolution in response to less extreme, but still 1–2 orders of magnitude, velocity step decreases in the laboratory demonstrates strengthening over a characteristic slip distance independent of the final slip rate, a feature consistent with the slip dependence of friction predicted by the Slip formulation (22, 23). Therefore, somewhat paradoxically, while load-point holds and large velocity-step decreases both probe the evolution of friction following large reductions in slip rate, the traditional interpretations of these two protocols seem to provide entirely contradicting versions of the processes underlying frictional strengthening.

One resolution to this paradox is to hypothesize a rate-sensitive transition from slip- to time-dependent strengthening that is hidden within the orders-of-magnitude gap in the slip rates typically probed by these two sliding protocols (24). To test this hypothesis, and to eliminate any effects of differences in samples or experimental conditions, we ran a suite of extremely large velocity step decreases (0.5 to 3.5 orders of magnitude between $3\,\mu\mathrm{ms}^{-1}$ and $0.001\,\mu\mathrm{ms}^{-1}$) and load-point holds (of durations $10 - 10^4$ s) on an initially bare granite sample, all during the same experimental run. For our experimental conditions, these extreme velocity step decreases reach slip rates as low as those accessed during hold durations of a few 100 s – durations comfortably larger than those above which time-dependent strengthening has been widely inferred (4, 5, 11). Crucially, this means that the data from either the velocity-step or slide-hold protocols are independently sufficient to test for a rate-sensitive transition from slip- to time-dependent strengthening with decreasing slip speed.

Contrary to conventional wisdom, we find that data derived from both sliding protocols support dominantly slip dependent strength evolution, even for nearly stationary surfaces (minimum estimated slip speeds $< 10^{-5}\mu$m/s). In particular, we find that the Slip equation describes most of the data quite well using nearly identical parameters, even across these many orders-of-magnitude variations in slip rate. In contrast, the Aging equation produces worse fits to the data while also requiring orders-of-magnitude variations in the inferred RSF parameters across the diverse sliding conditions. We trace these failures of the Aging equation back to one central flaw – its prediction that strength increases primarily with time and not slip following large, rapid decreases in slip rate.

Rate-State friction and probing strengthening with velocity steps and holds

Within the RSF framework (1, 5, 9, 20, 25), the friction coefficient is expressed as a function of the sliding rate (V) and the 'state variable' (θ) describing the state of the sliding surface. In its simplest form the friction equation is:

$$\mu = \frac{\tau_f}{\sigma} = \mu_* + a \ln\left(\frac{V}{V_*}\right) + b \ln\left(\frac{V_*\theta}{D_c}\right), \qquad [1]$$

where μ is the friction coefficient, τ_f is the shear stress during sliding, σ is the normal stress, and the parameters a and b determine the amplitude of the log velocity and log state dependence of friction. μ_* is the steady-state friction value at an aribtrary reference sliding speed V_*. At moderate temperatures a and b are of order 0.01 (26), much smaller than the nominal friction value μ_* of $\sim 0.6 - 0.8$. Despite being small, the rate- and state-dependence of friction is important; it determines, for example, whether surfaces slide stably at the applied loading rate ($a > b$, referred to as "velocity-strengthening"), or potentially undergo stick-slip motion ($a < b$, "velocity-weakening"). The velocity dependence is universally positive ($a > 0$) and is generally interpreted to result from a thermally-activated Arrhenius process associated with breaking chemical bonds between asperities that bridge the sliding surface (27, 28). The source of the state-dependence is poorly understood. Despite apparent similarities in the phenomenology of state evolution among many classes of solids, including rock, glass, metal, paperboard, wood, plastics and rubber (6, 8, 10, 16, 18), it is not at all obvious that the physical and chemical processes underlying this evolution are shared.

It is commonly assumed that the time derivative of the state variable, $\dot{\theta}$, can be written as functions of the current values of V and θ only, although this assumption might be somewhat restrictive (20). For decades the most widely used forms of the state evolution equations have been:

$$\text{Aging (Dieterich) Equation}: \dot{\theta} = 1 - \frac{V\theta}{D_c} \qquad [2a]$$

$$\text{Slip (Ruina) Equation}: \dot{\theta} = -\frac{V\theta}{D_c} \ln\left(\frac{V\theta}{D_c}\right) \qquad [2b]$$

where D_c is a characteristic slip scale, often associated with the size of contacting asperities on the interface (2, 20). State here has units of time.

At steady-state sliding ($\dot{\theta} = 0$), both equations yield $V\theta/D_c = 1$, or $\theta = D_c/V$, consistent with the interpretation that at steady-state θ reflects 'contact age'. For both equations, $V\theta/D_c < 1$ leads to $\dot{\theta} > 0$. We refer to this as being 'below steady state'. The increase in friction resulting from the below-steady-state increase in θ is what we mean by frictional strengthening.

The Aging and Slip formulations differ in their predictions for strengthening when $V\theta/D_c$ drops to values much smaller than 1. Given that neither equation allows for instantaneous changes in state, such 'far below steady state' regimes can be attained via sufficiently large and rapid reductions in slip rate from steady-state sliding. In response, state evolution under the Aging formulation loses all sensitivity to slip rate, as Eq. (2a) reduces to $\dot{\theta} \sim 1$. State then evolves purely as a function of time, and again invites the interpretation that state is contact age. Note that cessation of slip is not

required to satisfy $\dot{\theta} \sim 1$; it is sufficient that $\theta \ll D_c/V$. In contrast, under the Slip formulation the rate of state evolution decreases to progressively smaller values as the size of the velocity reduction increases, with no strengthening in the limit $V \to 0$. Nevertheless, in practice, due to the finite compliance of testing machines, slip speed never decays to zero. Under these circumstances, both formulations predict an approximately logarithmic-in-time increase in frictional strength during long-duration load-point holds (strictly so under the Aging formulation, as $\dot{\theta} \sim 1$) (20, 23).

Therefore, that frictional strength increases nearly logarithmically with hold duration in slide-hold-slide experiments does not by itself distinguish between evolution of friction with slip or with elapsed time.

The slip sensitivity of strengthening was explored by Beeler et al. (4) in an experiment consisting of the same sequence of holds at two very different machine stiffnesses. They showed that the rate of increase in peak friction with log hold duration was independent of the adopted stiffness, and hence independent of the very different amounts of slip that accrued during the holds. Beeler et al. interpreted these data as supporting time-dependent strengthening during holds. Together with the discovery of logarithmic-in-time contact area growth (10, 11), and the correpsondence between Aging-law-style time-dependent strengthening and contact area growth when viewed within the Bowden-Tabor picture (8, 13), the experiments of Beeler et al (4) have been cited as evidence in support of time-dependent contact-area growth leading to frictional strengthening during holds.

The strongest evidence against this viewpoint, and for the importance of slip in determining friction evolution far below steady state, comes from velocity step experiments as mentioned before. The Slip formulation, in fact, was introduced because it matches so well the results of laboratory velocity-step experiments, where friction is observed to approach its future steady-state value as roughly a decaying exponential over a characteristic slip distance (D_c), independent of the final slip speed as well as the magnitude and sign of the velocity step (20). For velocity step decreases this clearly calls into question the universality of the hypothesis that frictional strengthening far below steady state depends upon time rather than slip.

Recently, Bhattacharya et al. (23) resolved some of this conundrum by reinterpreting the slide-hold-reslide experiments of Beeler et al. Bhattacharya et al. showed that the Slip formulation can model the stiffness-independence of the healing rate inferred from the peak friction data as well as the Aging formulation, albeit over a narrower range of parameter values. Moreover, the holds preceding these peak friction values exhibit strongly stiffness-dependent stress relaxation rates which, with constant RSF parameters, cannot be captured by the Aging formulation but are well modeled by the Slip formulation. However, this does not rule out the possibility that this apparent failure of the Aging formulation has nothing to do with the prescription of state evolution, and is, instead, just an artifact of the assumption of velocity-independent RSF parameters. To explore the latter possibility, it is necessary to increase the size of the velocity-step decreases, and drop the target velocity into the range accessed by moderately long holds. This will effectively allow any rate-dependence of the RSF parameters to be detected by the rate steps alone. The Tullis rotary shear apparatus at Brown University (25, 29, 30) is uniquely suited to our purpose given that it can be servo-controlled using a resolver near the sliding interface to artificially stiffen the machine to around 30-40 times its natural stiffness (4, 23). All the experiments reported in this paper make use of this stiffened setting. Increasing the apparatus stiffness ensures that a large velocity step imposed at the load point is translated to the sample with greater fidelity. This maximizes the departure from steady state for a given velocity step decrease at the load point (31), which facilitates distinguishing slip-from time-dependence when inverting the resulting friction data.

As we will show, the dataset generated from the experiments described herein provide sufficient diagnostic power to join a growing body of work, referenced later, suggesting that (1) frictional "state" is not synonymous with contact area, and (2) slip is essential to frictional strengthening as observed in the laboratory.

Large velocity-step decreases on a stiff apparatus. The velocity steps were carried out at 25 MPa normal stress on a hollow, cylindrical sample of Westerly granite with outer and inner diameters of 54 and 44 mm (for details of the apparatus and sample see *SI Appendix* and Figures S2 and S3). The sample was initially ground flat and then roughened at a fine scale using 60 grit grinding compound. We report experimental results only after about 120 mm of slip. At these large values, the sample reached a stable, quasi-constant, steady-state velocity weakening value of $a-b \approx -0.003$ (Figure S6). Previous studies on the same apparatus under similar conditions have shown that, during the accumulation of $\sim 40-100$ mm of slip, a 70-100 μm thick layer of gouge develops on Westerly granite samples, with the total shear being accommodated in a narrow (20-30 μm wide), quasi-planar, shear zone within this gouge (29).

To estimate the slip velocity from the displacement measured by the resolver (what we term the 'load point'), we must correct for elastic deformation of the intervening material (about 5 mm of rock plus a thin layer of glue). The elastic stiffness k (expressed as friction change per differential slip distance between the surface and the load point) was determined to be 0.065 μm^{-1} (see *Materials and Methods* and *SI Appendix*, Figure S4). Assuming homogeneous shear stress and slip distribution on the sliding interface, the elastic relation between the measured shear traction on the sample (τ), the load-point displacement ($\delta_{\rm lp}$), and the surface slip (δ), is

$$\tau = k\sigma(\delta_{\rm lp} - \delta), \qquad [3]$$

Taking the time-derivative enables us to estimate the slip speed V in terms of the servo-controlled load-point velocity V_{lp} and the time-derivative of the shear load:

$$V = V_{\rm lp} - \frac{\dot{\tau}}{k\sigma}. \qquad [4]$$

Because the surface is always sliding, even at the end of the longest load-point holds ($V = 0.02 \pm 5\%$ nm s^{-1} at the end of our 10000s holds; see *SI Appendix Figure S5*), and because slip speeds and accelerations are small enough that inertia is negligible, we can relate changes in friction to changes in shear load throughout these experiments via $\Delta\mu = \Delta\tau/\sigma$.

Figure 1A shows friction data from a large number of velocity-step decreases and increases. In these tests, the sample

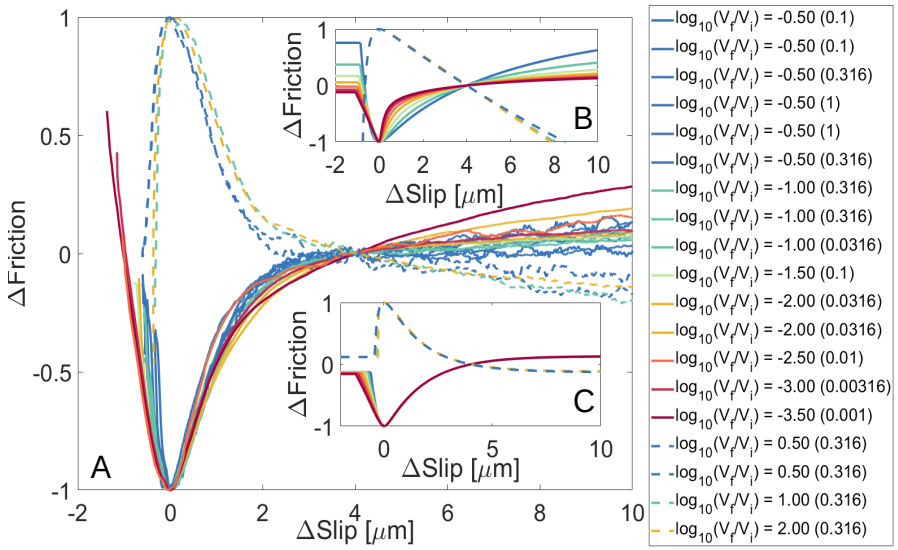

Fig. 1. (A) Large velocity-step decreases and increases on initially bare granite. Beyond 120 mm of total slip, 16 velocity-step decreases and 13 increases were carried out spanning 0.5-3.5 orders of magnitude. This plot shows 15 of these step decreases and 4 of the increases; the remainder are shown in Figure S18. The legend shows $\log_{10}(V_f/V_i)$ values coded by color; in parentheses are the final slip speeds V_f in μm/s. The slip is set to zero at the stress minimum (or maximum for the step increases). The data are smoothed over $0.2\,\mu$m for the step downs and over $0.4\,\mu$m for the step ups. The main panel shows the friction normalized by its change between 0 and $4\,\mu$m of slip. (B) and (C) show the evolution of friction for the range of step increases and decreases shown in A (colors denote step-sizes as in A) for the Aging and Slip formulations respectively. The changes in friction are measured from its value at 4μm and are normalized by the maximum amplitude of this change, as in (A). The parameters used for the Aging and Slip simulations are derived from fitting the velocity-step decreases (see *SI Appendix* and Table 1). The modeled time series is smoothed identically to the data. In (A), the friction values for the two largest step decreases begin well above zero because of the normalization scheme (the friction by 4 μm of slip remains well below its future steady state value; see Figure 2).

is initially run to steady state at a velocity $V_{lp} = V_i$, and then V_{lp} is changed to V_f over ∼0.02 s. When servo-controlling off the near-fault resolver we are able to impose sliding rates of 3 to $0.001\mu\text{ms}^{-1}$, allowing velocity jumps of up to 3.5 orders of magnitude. Previously published jumps have been limited to 2 orders of magnitude.

Each friction curve in Figure 1A has been normalized by the amplitude of its total change from its extremum to its value measured at $4\,\mu$m of slip, with slip defined as zero at the extremum. Over this initial $4\,\mu$m post-minimum slip, the plot clearly shows that frictional strength evolves over a length scale that is independent of both the step size and final slip speed V_f.

For comparison, we have plotted numerical simulations of velocity-step decreases using both the Aging formulation (Figure 1B) and the Slip formulation (Figure 1C). These simulations were run with the appropriate stiffness and a, b and D_c values derived by fitting the first 3 μm of the post-step friction evolution from a subset of the velocity steps shown in Figure 1A (see *Materials and Methods* and *SI Appendix*, Figures S6, S7 and S8).

Note, that in both the observations and the simulations, after a step decrease in V_{lp}, the stress first decreases to a minimum before increasing to its future steady-state value at $V = V_f$. In the simulations, the steep stress decay prior to the minimum is dominated by changes in the $a\ln(V/V_*)$ term in (1) (a rapid velocity drop at relatively constant state), whereas the subsequent steep stress increase is dominated by changes in the $b\ln(V_*\theta/D_c)$ term (state increases at nearly constant $V = V_f$; see *SI Appendix*, Figure S7). Therefore, across the many order-of-magnitude slip rate variations in Figure 1A, friction evolution for the first 4 μm of slip following the stress minimum represents frictional strengthening over elapsed times that vary by more than three orders of magnitude. This suggests that the collapse (for these short slip distances) of the whole suite of post-minimum velocity step data onto nearly the same curve implies the primacy of interfacial slip accumulation over time elapsed in determining this strengthening. The Slip formulation inherently captures this phenomenology, given its prediction that friction evolves to steady state over a characteristic slip scale, independent of the step size and V_f (20) (Figure 1C).

On the other hand, following a large velocity-step decrease, the Aging formulation predicts strengthening over length scales that decrease dramatically as the size of the velocity step increases (note this feature in the progression of colors subsequent to the stress minimum in Figure 1B). For velocity decreases that push the interface far below steady state ($V\theta/D_c \ll 1$), the rate of friction change with slip $d\mu/d\delta$ increases almost as rapidly with increasing velocity reduction as the velocity ratio V_i/V_f (*SI Appendix* and Figure S12). This is in clear contradiction with the data.

The velocity step data from Figure 1 are shown again as non-normalized friction versus slip in Figure 2A, with the changes in friction referenced to the pre-step steady-state level. The corresponding simulation results using the Aging and Slip formulations are shown in Figures 2D and 2E. Notably, for the experimental data the amplitude of the stress minimum $\Delta\mu_{\min}$ increases linearly with the logarithm of the size of the velocity step (inset in Figure 2A), with a slope of around -0.01. Using parameters derived from fits to the velocity-step decreases (Table 1), Slip formulation simulations also show a linear growth in $\Delta\mu_{\min}$ with log step size with a slope ~ -0.009 (Figure 2C). The data also show (Figure 2A and Figure S13 in *SI Appendix*) that the slip accumulated between the start of the velocity step and the friction minimum increases quasi-linearly with the log of the step size, again consistent with the Slip formulation simulations (Figure 2E).

The Aging formulation, on the other hand, predicts a non-linear relationship between $\Delta\mu_{\min}$ and log step size with the rate of increase in $\Delta\mu_{\min}$ decreasing systematically with larger steps (Figure 2B). In general, any increase in state (strengthening) between the onset of the velocity step and the friction minimum reduces the eventual amplitude of $\Delta\mu_{\min}$. For large velocity step decreases ($V_f/V_i \ll 1$), $V\theta/D_c \ll 1$ prior to the friction minimum. Under an Aging-style formulation this

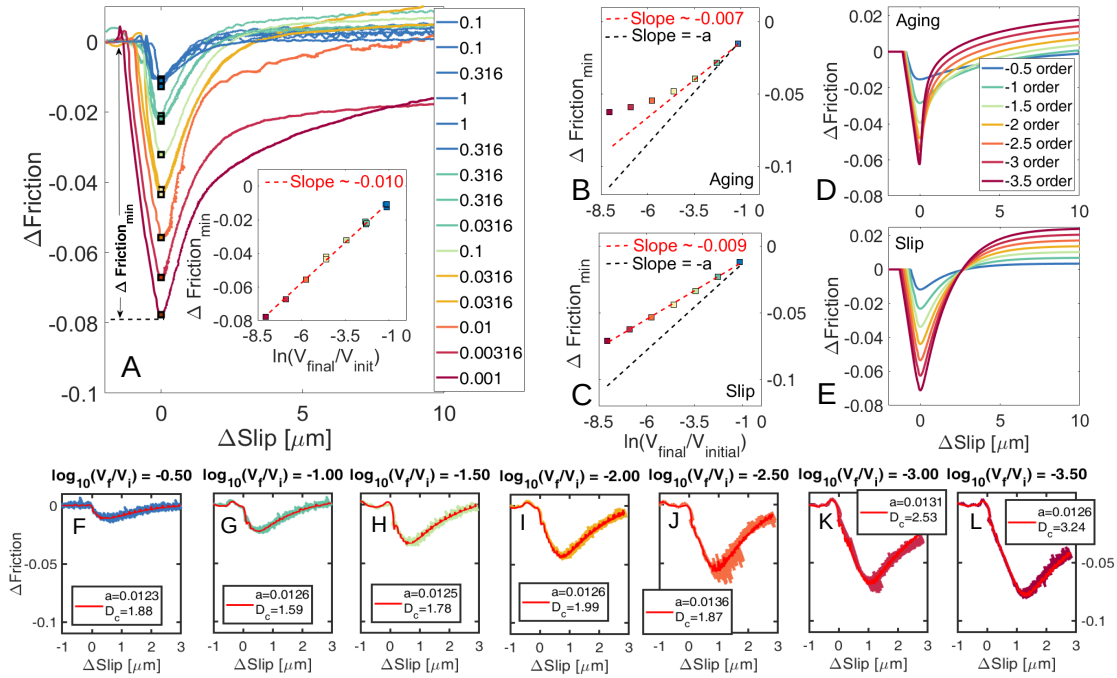

Fig. 2. (A) Same set of velocity step decreases as in Figure 1 color coded identically according to $\log_{10}(V_f/V_i)$, but plotted as non-normalized friction versus slip. The numbers in the legend show V_f in μms^{-1}. Slip is set to zero at minimum stress and shear stress is set to zero at the pre-step level. The data are smoothed as in Figure 1. Inset shows the evolution of the stress minimum ($\Delta\text{Friction}_{\text{min}}$) with log step size. (B) Stress minima following velocity-step decreases as a function of log step size, from the (smoothed) finite stiffness simulations in Figure 1B for the Aging formulation. (C) Same as (B) but for the Slip formulation. Note that the Slip formulation predicts linear evolution of the stress minima with log step size, while the Aging formulation predicts that the stress minima deviate to significantly shallower values from the initial linear trend as step size increases, due to increased state evolution. The black dashed lines in (B) and (C) have the slope of $a = 0.0144$ for the Aging and $a = 0.013$ for the Slip formulation. The trend of the stress minima from the data in (A) is linear, as predicted by the Slip formulation. (D) and (E) show the evolution of friction for the Aging and Slip simulations of Figures 1B and 1C, respectively, but referenced to the pre-step steady value as in 2A. (F)-(L) show Slip formulation fits to one step of each size. These fits are allowed to use different a and D_c ($a - b$ for each is fixed at -0.003), and are a subset of the fits to all the step decreases in Figure S8. Note the similarity in inferred a and D_c values across the steps and the excellent fit to the data.

leads to $\dot{\theta} \sim 1$ and a much larger increase in θ prior to the friction minimum than for the Slip formulation. This leads to considerable shallowing of the curve of $\Delta\mu_{\text{min}}$ with decreasing V_f/V_i.

Figures 2F-L show Slip formulation fits to the first 3 μm of post-step friction evolution of one each of the different step sizes in our experimental suite (all steps are fit in Figure S9). Unlike the fits used to infer the RSF parameters for the simulations in Figures 1C, 2C and 2E, the fits in Figures 2F-L allow different values of a and D_c (while fixing $a - b = -0.003$) for every velocity step shown in Figure 1A. These fits reveal that the Slip formulation requires almost no variation in a, and D_c variations of less than a factor of 2, to fit the whole suite of velocity step decreases equally well. To the extent that the larger values of D_c for the two largest velocity steps might be statistically meaningful, note that this would imply an even slower rate of fault strengthening with slip for the largest velocity reductions, whereas time-dependent strengthening requires the opposite. However, the 95% confidence intervals shown in Figure S11 seem to allow the possibility that any trends in D_c with step size are not significant.

While we have thus far focused on state evolution in response to velocity-step decreases, for completeness we point out that the velocity-step increases in Figure 1A also show systematic support for the Slip formulation. The data exhibit a quasi-characteristic length scale for stress evolution following the friction peak, independent of the sign as well as the size of the velocity step – a feature consistent with the Slip formulation (Figure 1C) (28, 32–34). The Aging formulation, in contrast, predicts linear slip weakening post-peak for velocity-step increases that push the sliding surface far above steady state ($V\theta/D_c \gg 1$) (28, 35) (see Fig. 1B). Further, since the amplitude of the friction peak increases with step size, a constant rate of weakening implies that steady state friction is attained over slip distances that also increase with step size – opposite to the trend predicted for step decreases. It is well established that such asymmetry in the frictional response between large velocity step increases and decreases is not supported by experiments (20, 22, 25, 28, 32, 36) and neither is it seen in our data.

Before concluding this section, we point out that most of our velocity step increases and decreases show a long-term evolution in stress over slip distances much larger than the D_c derived by fitting the first few microns of slip following the step. Neither the Aging nor the Slip formulation can capture this feature with a single state variable (20, 25). This is the main reason we avoid fitting more than the first 3 microns of slip following the step with our one state variable models (see *Materials and Methods*). Note that in obtaining the value $a - b = -0.003$ (supplementary Figure S6), we use the steady state values at more than 50μm of slip following our velocity steps. This value of $a - b$ probably corresponds better to a two state variable picture (25). But, on the other hand, the joint fit to the velocity steps in supplementary Figure S7,

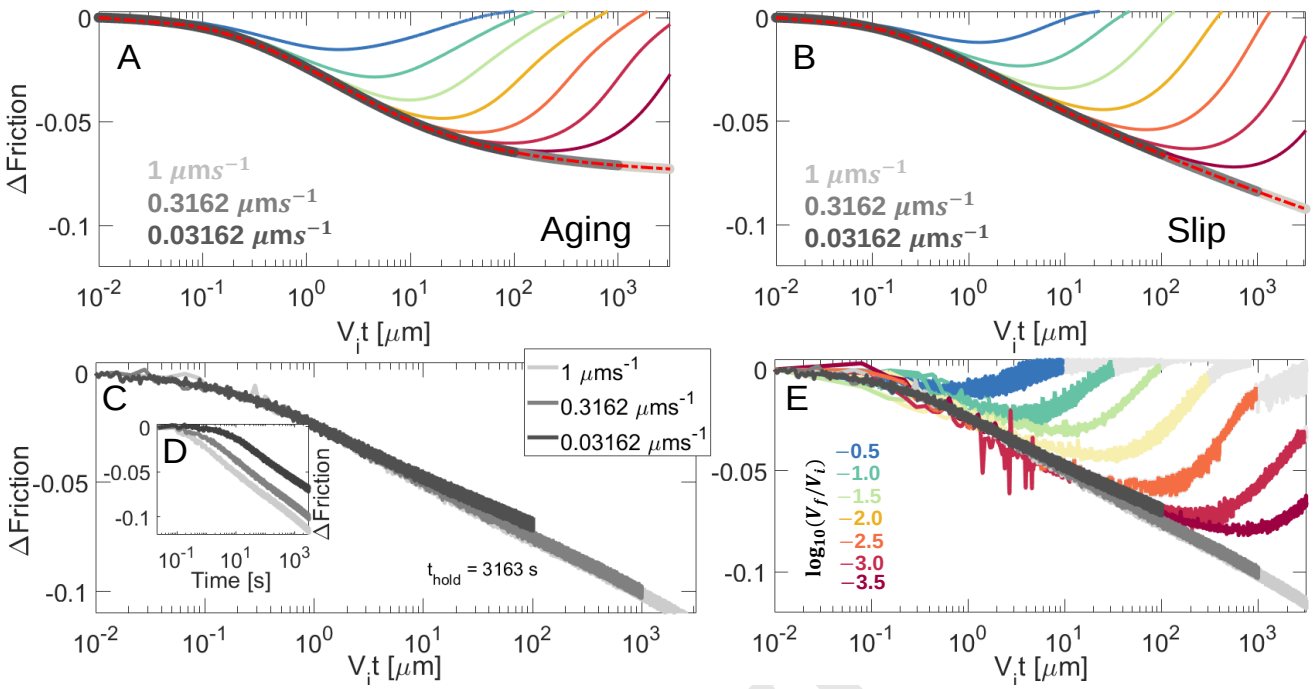

Fig. 3. Changes in friction, referenced to the prior steady-state value at slip speed V_i, for velocity-step decreases (solid colored lines) and holds (gray lines and dashed red line). Solid colored lines in (A) show the same finite stiffness simulations for the Aging formulation as in Figure 1B, now plotted vs. the logarithm of scaled time $V_i t$. The dashed red curve shows the stress relaxation trajectories of a 3000s hold with $V_i = 3\mu\text{ms}^{-1}$ and the same a, b and D_c as the velocity steps. The gray curves are for the same parameters as the red dashed curve except for the different indicated V_i. (B) is the same as (A), but for the Slip formulation with its corresponding velocity-step-derived RSF parameters. (C) shows that the friction evolution during laboratory holds of 3163 s at 3 different initial slip speeds from 0.03 to 1 μm/s collapse onto nearly the same trajectory when plotted vs. log scaled time $V_i t$. (D) shows the same data when plotted as function of time. (E) shows the same hold data and all the velocity step-decrease data of Figures (1) and (2), using the same scaling of time and color scheme as panels (A) and (B).

using the Slip formulation with a single state variable, requires $a - b = -0.003$ without any a priori constraints. Given this, and for its analytical simplicity, we have restricted ourselves to the one-state-variable picture.

In summary, the fact that the data from far below steady state – both the pre-minimum stress decrease and the post-minimum increase – are so consistent with the Slip formulation over the first few microns of slip, where (for all but the largest step) most of the post-minimum stress increase occurs, indicates that slip-dependent strengthening is responsible for most of the state evolution observed in these data. And, even when the data deviate from single-state-variable Slip formulation predictions, as do the two largest step decreases, they do so by strengthening less rapidly with slip than predicted (see also Figure S6). This is still inconsistent with time-dependent strengthening, which predicts more rapid strengthening with slip in response to larger step decreases (see *SI appendix*).

Comparing holds to the large velocity-step decreases. Our study stands apart from previous work in that it analyzes velocity step decreases and holds within a unified framework. For this reason it is useful to examine the extent to which our largest velocity step decreases and holds access similar sliding conditions. In Figure 3 we compare the stress evolution in laboratory and simulated velocity-step decreases (solid colored lines) to that in holds (gray lines). Figures 3A-B show numerical simulations comparing the shear stress relaxation during ∼3000s holds from the different laboratory pre-hold driving rates we used ($V_i = 1$, 0.3 and 0.03 μms^{-1}), to the shear stress evolution following the different laboratory velocity step sizes.

In Figures 3C-E we show corresponding laboratory hold and velocity-step data with Figure 3E being the analog of Figures 3A and B.

The simulations show that most of the stress decrease between the onset of the velocity steps and the subsequent friction minimum follows the stress relaxation trajectory of the different load point holds, when the data are plotted against rescaled time $V_i t$. This scaling removes any dependence of friction evolution on V_i, within the traditional RSF framework (i.e., constant a, b and D_c with no intrinsic velocity scale; see *Materials and Methods*) (37, 38). Figure 3C applies the same scaling to data from three ∼3000s holds initiated at different V_i (Figure 3D), and Figure 3E adds to this to all the velocity steps from Figure 1A. Note that the measured stress relaxations across the entire suite of holds (gray curves) also collapse to a single trajectory in Figures 3C and 3D. This is a significant result, as it provides no evidence for the hypothesis that the RSF parameters values change substantially at sliding velocities intermediate between V_i and the velocities reached by the ends of the holds (see *Materials and Methods*).

Figures 3B and E show that the velocity steps and holds share friction phenomenology down to slip rates as low as that of the largest velocity step decreases ($\sim 10^{-3}\mu\text{ms}^{-1}$). The longest holds then extend the slip rates accessed to values below $10^{-5}\mu\text{ms}^{-1}$. We show in the following section that these holds are fit well by the Slip formulation, using parameters very similar to those inferred from the velocity steps. Figure S15A shows that, for the Slip formulation, the largest velocity steps in our experiments access the same slip rates as holds of a few hundred seconds in duration irrespective of their pre-hold

sliding rates. This shows the utility of the large velocity-step decreases in our experiments – they clearly exhibit slip-dependent healing at the same sliding velocities achieved in holds long enough to clearly show logarithmic-in-time growth of both peak friction (4, 5) and contact area (10, 11).

Slide-hold experiments. Fits to our hold data (shown in Figure 4) are all constrained with $a - b = -0.003$, as determined from the steady-state friction value as a function of sliding speed (*SI Appendix* Figure S6). Holds of all durations from a particular V_i were fit jointly. The only exception are those with with $V_i = 1\mu\text{ms}^{-1}$ (Figures 4C and F), where we do not fit the two longest holds. For unknown reasons, and unlike the holds with $V_i \sim 0.3$ and 0.03 μms^{-1}in the other panels, the longer holds with $V_i = 1\mu\text{ms}^{-1}$ do not track the trajectories of the nominally identical shorter holds over their shared duration. Figures 4A-C show fits using the Aging formulation. Although the fits up to modest values of $V_i t$ ($\lesssim 10^2$) appear not too bad, they require values of D_c orders of magnitude larger than those inferred from the velocity steps (Table 1). To rationalize this feature of the fits, we note that under an Aging formulation with $a < b$, the rate of shear stress relaxation in response to a load point hold, $d\tau/d\log(t)$, decreases with time, ultimately vanishing in the limit $V_i t \gg D_c$ (23). This is a direct implication of time-dependent strengthening ($\dot{\theta} \sim 1$ far below steady state), and can be viewed as the 'infinitely large step' limit of the pronounced shallowing of the friction minima with increasing step size already seen in Figure 2B. For $a - b = -0.003$, the Aging formulation predicts that the shear stress decay during holds begins to significantly shallow for $V_i t/D_c \gtrsim 2$, or $V_i t \gtrsim 20$ for $D_c \sim 10\mu$m (Figure 3A). The hold data, however, show nearly log-linear stress relaxation for hold durations orders of magnitude larger than this. Therefore, an Aging formulation with $a < b$ can produce good fits to these hold sequences only by requiring that D_c be not much smaller than the values of $V_i t$ accessed during these holds.

The inset in Figure 4A shows the distribution of D_c values estimated using a Monte Carlo inversion method (see *Methods and Materials*), obtained by fitting each of the three holds in the sequence individually. The inferred values of D_c increase with hold duration t_{hold}, as expected to satisfy the requirement that $V_i t_{\text{hold}}$ not be much larger than D_c. For the same reason, the inferred values of D_c increase with V_i when fitting holds of the same duration in Figures 4A–C (Table 1; the only exception to the latter statement is a second set of holds with $V_i = 0.316\,\mu\text{ms}^{-1}$ shown in Figures S16B and C).

To further evaluate the suitability of the Aging formulation to model these data, we utilize the velocity-weakening fit to the velocity steps obtained from the Aging formulation to numerically predict the stress relaxation during the longest hold in each panel (dashed orange lines in Figures 4A-C). These numerical predictions significantly underestimate the shear stress decrease observed during the longer holds. This is expected, given the velocity steps are equivalent to hold durations much shorter than the longest holds at each V_i (for relevant Aging equation predictions see Figure S14A).

In contrast to the Aging formulation, the Slip formulation fits these holds very well (Figures 4D-F) with parameters nearly identical to those inferred from the velocity steps (Table 1). For the sets of holds in Figures 4D-E, these Slip equation fits capture the observed stress relaxation across the whole range of hold durations equally well with the same set of parameters. This is formally shown in the inset of Figure 4D, where it can be seen that, in contrast to the Aging formulation, the distribution of acceptable values of D_c inferred by fitting each of the three holds in the sequence individually are statistically equivalent. For the set of holds in Figure 4F, as noted previously only the three shortest holds were fit. The D_c inferred from this set of holds is about twice as large as those in panels D and E, within the range of variation in D_c inferred when all the velocity steps are fit independently.

So, overall, and consistent with the findings of (23), the Slip equation fits to the internally consistent holds in Figures 4D-E capture the stress relaxation at the longest hold times better than the corresponding Aging equation fits. The good Slip equation fit to the shear stress data at such low slip rates (as low as 0.02 nms^{-1}; see Figure S5) implies, remarkably, that state evolution in these experiments is controlled by slip rather than elapsed time even at rates more than an order of magnitude below plate tectonic rates.

Before finishing this discussion, we point out that, unlike the holds, the corresponding reslides are not well modeled by either the Slip or the Aging formulation (Figures S17 and S18). For example, the Slip equation fits to the holds in Figures 4D-F both under-predict the static friction peaks upon resliding, and fail to capture the post-peak strength evolution (red curves in Figures S17 A-D). Therefore, neither of these widely used empirical formulations fit the entire range of laboratory data equally well.

Discussion

The main goal of this work was to determine whether the frictional strengthening of surfaces sliding at conditions far below steady state is dominantly slip-dependent or time-dependent. For both velocity step decreases and slide-hold laboratory protocols we have established that the surface strengthens (that is, state increases) primarily with slip. In doing so, we have also demonstrated that the conventional (but self-contradictory) wisdom that state evolution in response to velocity-step decreases is slip-dependent, while that in response to load-point holds is time-dependent, is incorrect. Instead, by treating holds as the limit of increasingly large velocity step decreases, we have shown that the phenomenology of frictional healing is not only slip-dependent but is well explained by the standard Slip formulation to within a few tens of percent of variation in the RSF parameters. This consistency is observed across more than 5 orders of magnitude in slip rates, from $3\mu\text{ms}^{-1}$ to $< 10^{-5}\mu\text{ms}^{-1}$.

In contrast, we have shown that any formulation in which the state contribution to friction increases as log time, analogously to the log-time contact area growth observed at low slip rates, makes the interface too strong to match the stress relaxation observed during both load-point holds and, prior to their stress minima, step velocity decreases. The Aging equation is a particular example of such a formulation.

In this context, it is worth remembering that log-time growth of contact area is not only well established in observations in transparent materials (10, 11), it also has a well-accepted theoretical basis (39). In rock, the same log-time growth of contact area has been inferred from proxy measurements of fault-normal displacement and acoustic transmissivity during load-point holds (31, 40) or from log-time compaction of granular wear material accumulated on initially bare rock in-

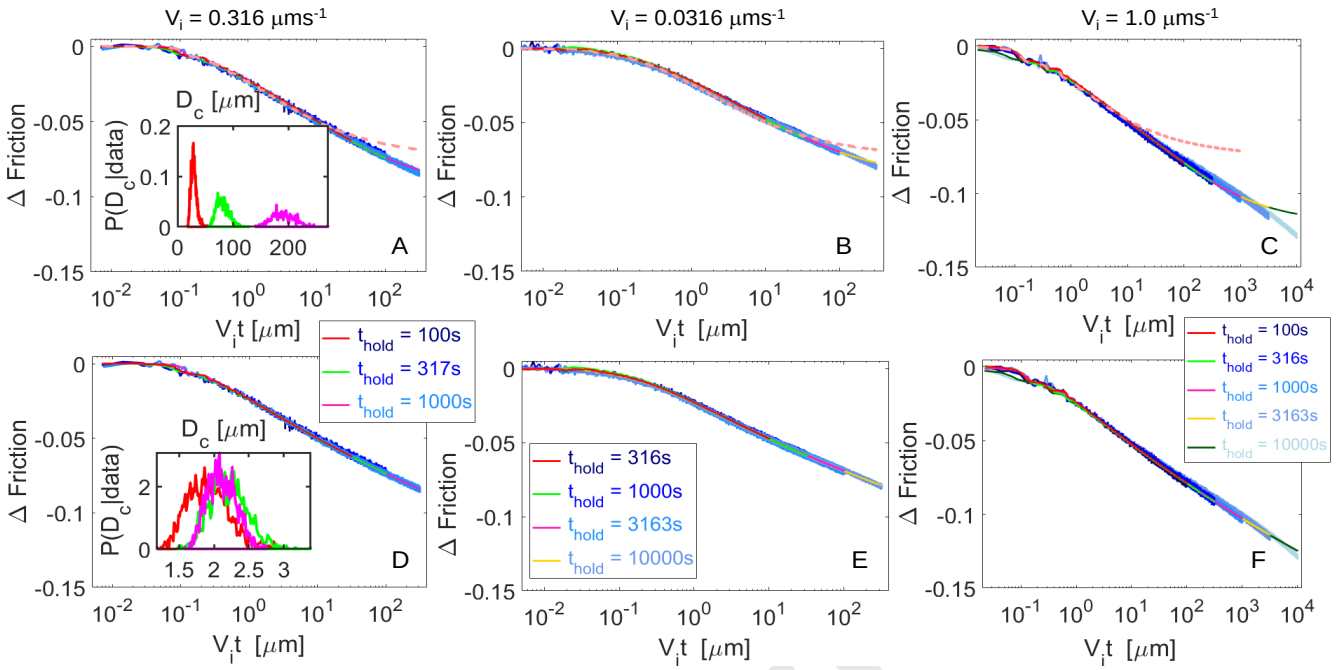

Fig. 4. Fits to the hold portions of the slide-hold-slide tests carried out during the same experimental run as the velocity steps in Figure 1. The data are represented in various shades of blue with lighter colors representing longer holds. The joint fits to all holds in each sequence are shown in the respective panels in colors other than blue. The friction change from the prior steady state is plotted as a function of scaled time $V_i t$ as in Figure 3. (A)-(C) Fits using the Aging formulation; note that these require unreasonably large values of D_c (Table 1). Dashed orange lines are predictions for the longest hold in the panel that was fit, using Aging parameters inferred from the velocity steps (see Table 1). (D)-(F) Fits to the same holds but now using the Slip formulation. The values of a and D_c required by the fits in (D) and (E) are nearly identical to those required to fit the velocity steps (Table 1 and Figure S3). The fit in (F) requires a D_c 65 % larger than that required to fit the velocity steps. The insets in (A) and (D) show the posterior distributions of D_c inferred from Monte Carlo inversions that fit the holds of different durations separately. Note that the Aging formulation requires progressively larger values of D_c for longer holds, while D_c inferred for the Slip formulation is statistically invariant across the range of hold durations. In Figures 4C and F ($V_i = 1.0$ μms^{-1}) we did not fit the two longest holds because they showed very atypical behavior – concave-down friction vs. log time curves at long hold times, and static friction peaks that decrease for hold durations longer than 10^3s (Figures 4F and S15).

Table 1. Rate-State parameters from fitting the friction data

Type	V_i	EE	TH	a	b	D_c	Fig#
Steps [a]	–	A	–	0.014	–	10.05	S4
Steps	–	A	–	0.022	0.018	0.99	S4
Holds [a]	0.032	A	10000s	0.012	–	84.85	4B
Holds [a]	0.32	A	1000s	0.013	–	103.40	4A
Holds [a]	0.32	A	3163s	0.012	–	3055.33	S16
Holds [a]	1.0	A	1000s	0.013	–	663.66	4C
Steps	–	S	–	0.013	0.016	2.07	S7
Holds [a]	0.032	S	10000s	0.014	–	1.99	4E
Holds [a]	0.32	S	1000s	0.015	–	2.10	4D
Holds [a]	0.32	S	3163s	0.014	–	4.63	S16
Holds [a]	1.0	S	1000s	0.015	–	3.43	4F

EE denotes choice of evolution equation – A for Aging, S for Slip.

TH denotes the longest hold duration fit as part of this series.

Fig# denotes the figure number for the listed fits.

V_i values in μms^{-1}, D_c in μm.

[a] denotes $a - b = -0.003$ constraint imposed on these fits.

terfaces (41). Therefore, it is quite remarkable how poorly the Aging formulation performs in reproducing friction evolution during holds, even though it mimics very well the observed phenomenology of contact area growth under similar conditions. Our results, thus, add to a growing body of evidence that the evolution of 'state' embodies more than just changes in contact area (42–45).

The bigger surprise is the extreme slip-sensitivity of friction at even sub-nanometric slip rates. Several underlying mechanisms could give rise to slip-dependent state evolution. Asperities might retain a memory of the velocity(ies) at which they formed, in which case reaching a new steady state might require swapping out the old contacts for the new, regardless of how long that takes (46). Additionally, contact area might grow during holds or normal stress increases, but that new contact area might have to undergo some strain-hardening (via slip) before reaching its steady-state strength (44). Although these ideas have been explored numerically (46, 47), no formulation developed thus far does better than the Slip formulation in describing lab friction data.

However, recent Discrete Element Method (DEM) simulations of a granular gouge layer sheared between two parallel plates, as a model for fault friction, behaved very similar to the Slip formulation with nearly constant RSF parameters during velocity-step and slide-hold protocols, consistent with laboratory experiments (48). The model gouge also underwent log-time compaction during the holds, meaning that the

DEM simulations share with lab experiments the property that although the interface normal displacements are seemingly consistent with the conventional understanding of the Aging formulation, the simulated shear stress decay follows the Slip formulation. Although these simulation results appear quite promising, the microscopic mechanisms giving rise to the macroscopically lab-like behavior remain unknown. However, granular systems are known to exhibit the same slow dynamics of other disordered systems near the 'glass transition temperature', behavior that has previously been invoked to explain non-monotonic contact area changes in PMMA at times of constant normal load (49).

It is possible, even likely, that at slip rates even lower than those accessed in our experiments, some additional process operates that involves time-dependent healing and also contributes to frictional strengthening. For example, it is known that interfaces continue to strengthen even when held truly stationary by unloading to zero shear stress (3, 6, 21, 50). It is also important to note that while the Slip formulation fits our velocity steps and holds with nearly identical parameters, it cannot fit well the peak friction upon resliding after the holds. This might indicate that the interface undergoes some additional physical change during the stress increase between the minimum at the end of the hold and the subsequent stress peak that is not captured by any existing state evolution formulation.

What also remains to be examined is the extent to which this phenomenology of rock friction extends to other materials. The clearest evidence for log-time contact area growth comes from transparent acrylic (PMMA), but PMMA samples have yet to be subjected to as exhaustive a set of sliding conditions as reported in this manuscript. This wide range of conditions has proven to be necessary to distinguish between time-dependent and slip-dependent strengthening for surfaces far below steady state. A comprehensive study of the universality of friction phenomenology among other important natural and industrial material is necessary, particularly given the diversity of materials and purposes across which RSF is used – elastomers to plastics/acrylics to metals to soft materials and micromachines (6, 15, 16, 51, 52).

Given that 'state' must in general depend upon both contact area and the quality of chemical bonding across those contacts (42, 43, 53, 54), it would be surprising if friction could be accurately described by a single state variable. It is thus remarkable that the empirical Slip formulation for state evolution does as well as it does, fitting velocity steps of both signs and load point holds with near identical parameters. This suggests that it is a good starting point for developing a state evolution formulation to better fit the reslides after holds. This is in contrast to earlier attempts at revising state evolution equations which considered time-dependent strengthening as embodied by the Aging formulation to be a desirable property of state evolution at low slip rates (24, 31). Our results, instead, show that this is the portion of the parameter space where time-dependent strengthening descriptions such as the Aging formulation are least compatible with laboratory friction data.

Materials and Methods

Estimating stiffness and $a-b$ from independent constraints. Our experiments were carried out on the Tullis rotary shear apparatus at Brown University, which was artificially stiffened using servo feedback from a near-fault transducer. To obtain an estimate of this higher stiffness, we used the initial loading curve of the reslides following a sequence of long holds carried out during the same experimental run. At the end of long holds, the block is sliding at rates orders of magnitude smaller than the pre-hold steady sliding rate V_i. Therefore, following the reslide, also at the rate V_i, there is an initial time window over which the slip rate of the block continues to satisfy $V \ll V_i$. During this initial portion of the reload, assuming quasi-static force balance between the driving shear stress and friction, we have

$$\Delta\mu = k(\delta_{lp} - \delta) = k\delta_{lp}\left(1 - \frac{\delta}{\delta_{lp}}\right) \approx k\delta_{lp}, \qquad [5]$$

where δ and δ_{lp} are surface and load point displacements since the reslide respectively, and initially $\delta/\delta_{lp} \ll 1$ for reslides following long holds. Note that k is the stiffness normalized by normal stress and $\Delta\mu$ is the change in friction. A linear fit to the $\Delta\mu$ vs. δ_{lp} plot over this initial portion following the reslide gives k as the slope (Figure S4). We use the reslides following a sequence of 3000 s and 10000 s holds carried out at three different values of V_i spanning more than an order of magnitude – 1, 0.3162 and 0.03162 μms^{-1}. For the linear fit, we chose one-seventh of the total number of points between the onset of the reslide and eventual peak strength to evaluate k. This fraction was chosen based on trial-and-error such that the spread in the estimated value of k was the least between our six chosen reslides. We found $k \sim 0.065\mu\text{m}^{-1}$ to be the mean stiffness from our fits.

For constant RSF parameters, the slope of the curve of steady-state friction vs. $\ln(V)$ is equal to $(a-b)$. In Figure S6 we show the estimation of $a-b$ from all the 0.5 to 2.0 order velocity steps in Figure 1A. The post-step steady state is chosen for all steps at 45 μm of post-minimum slip (brown stars in each panel). We did not use larger steps for $a-b$ estimation because of the prominent post-minimum transients present at 45 μm slip distance for these steps. We find that $a-b \sim -0.003$ explains the data well from the $3\mu ms^{-1}$ to $0.03\mu ms^{-1}$ slip rates covered between these steps.

Estimating a and D_c by fitting the velocity-step decreases. To constrain a and D_c, we fit either a representative size range of the velocity-step decreases (3.5-1 orders of magnitude) or all of the velocity steps in Figure 1A with the Slip equation. The forward model is simulated by equating the time derivative of $\Delta\mu$ in Eq. (5) (using the load point displacement history recorded during the experiment and $k = 0.065\mu\text{m}^{-1}$) with that in the friction law (Eq. (1)), with the Slip equation being used for state evolution (Eq. (2b)). All data are sampled uniformly at 50 Hz in these experiments. We fit the velocity step decreases in two ways – (i) parameters a, b and D_c are simultaneously and jointly inferred from all the velocity-step decreases shown in Figures S6 A-E, and (ii) parameters a and D_c are inferred independently by fitting all the velocity steps individually with the constraint that $a-b=-0.003$ (Figures S9 A-O). For the fits of type (i), we weight the misfit for each velocity step by the inverse of the total number of data samples in the fitting window to ensure that the data from all the velocity steps contribute equally to the aggregate misfit. For the inversion, we use an adaptive proposal, small-world, Markov chain Monte Carlo code. The algorithm and the general inversion procedure are described in the Supplementary materials accompanying (22). We minimize the weighted square root misfit between the modeled time series and the data at every time sample in the data. We model the evolution of friction only over the first 3 μm of slip after the onset of the velocity step. This avoids fitting secondary long term transients in the evolution of friction present in the data. For completeness, we carry out a set of Aging equation fits for all the velocity steps in Figure 1 jointly with the same a and D_c (see *SI Appendix* and Figure S8 for details). The inferred a and D_c values are reported in Table 1.

Scaling of friction response of holds and steps from different initial velocities under single-state variable RSF. Rate-state friction with constant parameter values and no intrinsic velocity scale predicts that friction evolution is independent of the pre-step or pre-hold

sliding rate V_i, when time is rescaled as $V_i t$. To show this, we begin by generalizing equation (1) to two state variables, and use V_i for the arbitrary reference velocity V_*:

$$\mu = \frac{\tau_f}{\sigma} = \mu_* + a \ln\left(\frac{V}{V_i}\right) + b_1 \ln\left(\frac{V_i\theta_1}{D_1}\right) + b_2 \ln\left(\frac{V_i\theta_2}{D_2}\right) \quad [6]$$

(extension to additional state variables is straightforward). We assume, as in equations (2), that the evolution equation for each θ_n can be expressed as a function of the dimensionless parameter $V\theta_n/D_n$:

$$\frac{d\theta_1}{dt} = F\left(\frac{V\theta_1}{D_1}\right) \; ; \quad \frac{d\theta_2}{dt} = F\left(\frac{V\theta_2}{D_2}\right). \quad [7]$$

To obtain an evolution equation for V following a velocity step or hold, dividing (3) by σ, equating this to the right hand side of (6), and taking the time derivative yields

$$\frac{dV}{dt} = V\frac{b_1}{a}\left[\frac{k}{b_1}\left(V_f - V\right) - \frac{\dot\theta_1}{\theta_1} - \frac{b_2}{b_1}\frac{\dot\theta_2}{\theta_2}\right], \quad [8]$$

where V_f is the post-step load-point velocity (zero for a hold). Next, we make (7) and (8) dimensionless by normalizing velocities by V_i and time (as well as θ_1 and θ_2) by D_1/V_i:

$$\frac{d\tilde\theta_1}{d\tilde t} = F\left(\tilde V\tilde\theta_1\right) \; ; \quad \frac{d\tilde\theta_2}{d\tilde t} = F\left(\tilde V\tilde\theta_2\frac{D_1}{D_2}\right); \quad [9]$$

$$\frac{d\tilde V}{d\tilde t} = \tilde V\frac{b_1}{a}\left[\frac{kD_1}{b_1}\left(\frac{V_f}{V_i} - \tilde V\right) - \frac{d\tilde\theta_1/d\tilde t}{\tilde\theta_1} - \frac{b_2}{b_1}\frac{d\tilde\theta_2/d\tilde t}{\tilde\theta_2}\right]; \quad [10]$$

where tildes represent dimensionless variables. Assuming steady-state sliding before the step/hold, the initial conditions on θ at the time of the step are

$$\tilde\theta_1\big|_{\tilde t=0} = 1 \; ; \quad \tilde\theta_2\big|_{\tilde t=0} = \frac{D_2}{D_1}. \quad [11]$$

Equations (9)–(11) show that, provided the RSF parameters a, b_n, and D_n are independent of sliding speed, $\tilde V(\tilde t)$ and $\tilde\theta_n(\tilde t)$ depend upon V_f/V_i (term in parentheses in (10)), but do not depend on V_i independently. Furthermore, taking the time-derivative of equation (3) and equating μ with τ/σ,

$$\frac{d\mu}{d(V_i t)} = k\left(\frac{V_f}{V_i} - \tilde V\right). \quad [12]$$

As both terms within the parentheses on the right side of (12) depend only upon V_f/V_i, again provided the RSF parameters are constant, plots of the friction change during holds should be independent of V_i when plotted vs. scaled time $V_i t$. In addition, velocity step decreases should be indistinguishable from holds as long as $V \gg V_f$. Thus, the generally clean overlap of the stress relaxation trajectories during the holds in Figure 3C is consistent with the RSF parameters being nearly constant across the > 5 orders of magnitude range of velocities accessed in these experiments.

ACKNOWLEDGMENTS. Financial support from two sources kept the Brown University lab operational during the time these experiments were conducted. Support derived from NSF grant number EAR1359596 and the Southern California Earthquake Center under grant 16026 (SCEC Contribution number 9952). SCEC is funded by NSF Cooperative agreement EAR-1600087 and USGS Cooperative Agreement G17AC00047. Support for AMR came from NSF grant number EAR1547286.

1. Dieterich JH (1972) Time-dependent friction in rocks. *J. Geophys. Res.* 77(20):3690–3697.
2. Dieterich JH (1978) Time-dependent friction and the mechanics of stick-slip. *Pure Appl. Geophys.* 116(4-5):790–806.
3. Nakatani M, Mochizuki H (1996) Effects of shear stress applied to surfaces in stationary contact on rock friction. *Geophys. Res. Lett.* 23(8):869–872.
4. Beeler N, Tullis TE, Weeks JD (1994) The roles of time and displacement in the evolution effect in rock friction. *Geophys. Res. Lett.* 21:1987–1990.
5. Marone C (1998) Laboratory derived fricition laws and their application to seismic faulting. *Annu. Rev. Earth Planet. Sci.* 26:643–696.
6. Berthoud P, Baumberger T, G'Sell C, Hiver JM (1999) Physical analysis of the state- and rate-dependent friction law: Static friction. *Phys. Rev. B* 59(22):14313–14327.
7. Karner SL, Marone C (2001) Frictional restrengthening in simulated fault gouge: Effect of shear load perturbations. *J. Geophys. Res.: Solid Earth* 106(B9):19319–19337.
8. Baumberger T, Caroli C (2006) Solid friction from stick-slip down to pinning and aging. *Adv. Phys.* 55(3-4):279–348.
9. Marone C (1998) The effect of loading rate on static friction and the rate of fault healing during the earthquake cycle. *Nature* 391:69–72.
10. Dieterich JH, Kilgore BD (1994) Direct observation of frictional contacts: New insights for state-dependent properties. *Pure Appl. Geophys.* 143:283–302.
11. Ben-David O, Rubinstein SM, Fineberg J (2010) Slip-stick and the evolution of frictional strength. *Nature* 463(7277):76–79.
12. Bowden FP, Tabor D (1964) *The Friction and Lubrication of Solids, Part 2*. (Oxford Univ. Press, New York).
13. Brechet Y, Estrin Y (1994) The effect of strain rate sensitivity on dynamic friction of metals. *Scripta Metall. Mater.* 30(11):1449 – 1454.
14. Dieterich JH (1979) Modeling of rock friction: 1. experimental results and constitutive equations. *J. Geophys. Res.* 84:2161–2168.
15. Prakash V (1998) Frictional response of sliding interfaces subjected to time varying normal pressures. *J. Tribol.* 120(1):97–102.
16. Ronsin O, Coeyrehourcq KL (2001) State, rate and temperature-dependent sliding friction of elastomers. *Proceedings of the Royal Society of London. Series A: Mathematical, Physical and Engineering Sciences* 457(2010):1277–1294.
17. Shroff SS, Ansari N, Robert Ashurst W, de Boer MP (2014) Rate-state friction in micro-electromechanical systems interfaces: Experiment and theory. *Journal of Applied Physics* 116(24):244902.
18. Heslot F, Baumberger T, Perrin B, Caroli B, Caroli C (1994) Creep, stick-slip, and dry-friction dynamics: Experiments and a heuristic model. *Phys. Rev. E* 49(6):4973–4988.
19. Carlson JM, Batista AA (1996) Constitutive relation for the friction between lubricated surfaces. *Phys. Rev. E* 53(4):4153–4165.
20. Ruina A (1983) Slip instability and state variable friction laws. *J. Geophys. Res.* 88:10,359–10,370.
21. Bureau L, Baumberger T, Caroli C (2002) Rheological aging and rejuvenation in solid friction contacts. *Eur. Phys. J. E: Soft Matter and Biological Physics* 8(3):331–337.
22. Bhattacharya P, Rubin AM, Bayart E, Savage HM, Marone C (2015) Critical evaluation of state evolution laws in rate and state friction: Fitting large velocity steps in simulated fault gouge with time-, slip-, and stress-dependent constitutive laws. *J. Geophys. Res.: Solid Earth* 120(9):6365–6385. 2015JB012437.
23. Bhattacharya P, Rubin AM, Beeler NM (2017) Does fault strengthening in laboratory rock friction experiments really depend primarily upon time and not slip? *J. Geophys. Res.: Solid Earth* 122(8):6389–6430. 2017JB013936.
24. Kato N, Tullis TE (2001) A composite rate- and state-dependent law for rock friction. *Geophys. Res. Lett.* 28(6):1103–1106.
25. Tullis TE, Weeks JD (1986) Constitutive behavior and stability of frictional sliding of granite. *Pure Appl. Geophys.* 124(3):383–414.
26. Blanpied ML, Marone CJ, Lockner DA, Byerlee JD, King DP (1998) Quantitative measure of the variation in fault rheology due to fluid-rock interactions. *J. Geophys. Res.* 103(B5):9691–9712.
27. Rice JR, Lapusta N, Ranjith K (2001) Rate and state dependent friction and the stability of sliding between elastically deformable solids. *Journal of the Mechanics and Physics of Solids* 49(9):1865 – 1898. The {JW} Hutchinson and {JR} Rice 60th Anniversary Issue.
28. Nakatani M (2001) Conceptual and physical clarification of rate and state friction: Frictional sliding as a thermally activated rheology. *J. Geophys. Res.* 106(B7):13,347–13,380.
29. Beeler NM, Tullis TE, Blanpied ML, Weeks JD (1996) Frictional behavior of large displacement experimental faults. *J. Geophys. Res.: Solid Earth* 101(B4):8697–8715.
30. Tullis TE (1997) Friction measurement apparatus in *Instruments of Science: An Historical Encyclopedia*, eds. Bud RF, Warner DJ. (Garland, New York), pp. 249–251.
31. Nagata K, Nakatani M, Yoshida S (2012) A revised rate- and state-dependent friction law obtained by constraining constitutive and evolution laws separately with laboratory data. *J. Geophys. Res.* 117:B02314.
32. Linker MF, Dieterich JH (1992) Effects of variable normal stress on rock friction: Observations and constitutive equations. *J. Geophys. Res.* 97(B4):4923–4940.
33. Rice JR (1993) Spatio-temporal complexity of slip on a fault. *J. Geophys. Res.* 98(B6):98859907.
34. Ampuero JP, Rubin AM (2008) Earthquake nucleation on rate and state faults – aging and slip laws. *J. Geophys. Res.* 113:B01302.
35. Rubin AM, Ampuero JP (2005) Earthquake nucleation on (aging) rate and state faults. *J. Geophys. Res.* 110:B11312.
36. Ruina A (1980) Ph.D. thesis (Division of Engineering, Brown University, Providence, Rhode Island).
37. Ranjith K, Rice J (1998) Stability of quasi-static slip in a single degree of freedom elastic system with rate and state dependent friction. *J. Mech. Phys. Sol.* 47(6):1207 – 1218.
38. Gu JC, Rice JR, Ruina AL, Tse ST (1984) Slip motion and stability of a single degree of freedom elastic system with rate and state dependent friction. *J. Mech. Phys. Sol.* 32(3):167 – 196.
39. Berthoud P, Baumberger T (1998) Shear stiffness of a solid–solid multicontact interface. *Proc. R. Soc. Lon. A: Mathematical, Physical and Engineering Sciences* 454(1974):1615–1634.
40. Nagata K, Kilgore BD, Beeler N, Nakatani M (2014) High-frequency imaging of elastic contrast and contact area with implications for naturally observed changes in fault properties. *J. of Geophys. Res.: Solid Earth* 119(7):5855–5875. 2014JB011014.
41. Beeler NM, Tullis TE (1997) The roles of time and displacement in velocity-dependent volumetric strain of fault zones. *J. Geophys. Res.: Solid Earth* 102(B10):22595–22609.
42. Li Q, Tullis TE, Goldsby D, Carpick RW (2011) Frictional ageing from interfacial bonding and the origins of rate and state friction. *Nature* 480(7376):233–236.
43. Thom CA, Carpick RW, Goldsby DL (2018) Constraints on the physical mechanism of frictional aging from nanoindentation. *Geophysical Research Letters* 45(24):13,306–13,311.

44. Kilgore BD, Lozos J, Beeler N, Oglesby D (2012) Laboratory observations of fault strength in response to changes in normal stress. *J. App. Mech.* 79(3):31007–1–31007–10.
45. Tullis TE, Bhattacharya P, Rubin A, Badt N, Beeler N (2020) Analysis of normal stress stepping experiments indicates that friction evolution depends on contact area quality rather than quantity in *AGU Fall Meeting*.
46. Li T, Rubin AM (2017) A microscopic model of rate and state friction evolution. *Journal of Geophysical Research: Solid Earth* 122(8):6431–6453.
47. Li T (2019) An effort to reconcile time- and slip-dependent friction evolution. *Journal of Geophysical Research: Solid Earth* 124(2):1838–1851.
48. Ferdowsi B, Rubin AM (2020) A granular physics-based view of fault friction experiments. *Journal of Geophysical Research: Solid Earth* 125(6):e2019JB019016. e2019JB019016 10.1029/2019JB019016.
49. Dillavou S, Rubinstein SM (2018) Nonmonotonic aging and memory in a frictional interface. *Phys. Rev. Lett.* 120(22):224101.
50. Karner SL, Marone C (1998) The effect of shear load on frictional healing in simulated fault gouge. *Geophysical Research Letters* 25(24):4561–4564.
51. Shroff SS, de Boer MP (2016) Full assessment of micromachine friction within the rate-state framework: Theory and validation. *Tribology Letters* 63(3):39.
52. Sahli R, et al. (2018) Evolution of real contact area under shear and the value of static friction of soft materials. *Proc. Nat. Acad. Sci.*
53. Weber B, Suhina T, Brouwer AM, Bonn D (2019) Frictional weakening of slip interfaces. *Science Advances* 5(4).
54. Tian K, Goldsby DL, Carpick RW (2018) Rate and state friction relation for nanoscale contacts: Thermally activated prandtl-tomlinson model with chemical aging. *Phys. Rev. Lett.* 120(18):186101.

PNAS
www.pnas.org

Supplementary Information for

The evolution of rock friction is more sensitive to slip than elapsed time, even at near-zero slip rates.

Pathikrit Bhattacharya, Allan M. Rubin, Terry E. Tullis, Nicholas M. Beeler and Keishi Okazaki

Pathikrit Bhattacharya.
E-mail: path_geoalum@alumni.princeton.edu

This PDF file includes:

Supplementary text
Figs. S1 to S19
References for SI reference citations

Supporting Information Text

1. Experimental apparatus and sample preparation

The friction experiments were performed on paired rings of Westerly granite using a gas-medium, high-pressure, rotary shear deformation apparatus at Brown University (Figure S2). The apparatus consists of a cylindrical pressure vessel, a pressure-generating system for confining pressure (Pc) and pore pressure (Pp), and axial and torsional loading systems (1–4). The torque (i.e., shear stress), the axial load, the axial shortening, and the rotation (i.e., shear displacement) are measured inside the pressure vessel nearby the sample rings (Figure S3). Therefore, frictional resistances from high pressure seals are not included for both stress and displacement measurements. The rotation is measured using a resolver with a digital 24-bit resolution per revolution pegging the resolution for the rotation of the sample at about 2×10^{-5} degree. This corresponds to a resolution of 9.2 nm on the recorded displacement with a circumferential sample length of 153.6 mm.

In this system, the axial load is controlled by a hydraulic servo-system. In addition, to minimize any elastic distortion being recorded as apparent slip during the velocity step, the torsional loading system is also controlled by a combination of hydraulic servo-system and an electro-hydraulic stepping motor with a feedback of the signal from the internal resolver for the shear displacement. This servo control system artificially increases the apparatus stiffness k more than an order of magnitude, depending on the experimental sample type, from about 0.0019 μm^{-1} (5, 6) to about 0.065 μm^{-1} (expressed as friction, i.e., shear stress/normal stress) at a normal stress of 25 MPa (Figure S4). This value implies that the elastic distortion by a change of shear stress $\Delta\tau$ of 2.5 MPa (equivalent to 0.1 change in friction at 25 MPa) is about 1.5 μm for the artifically stiffened experimental setup.

We used a block of Westerly granite (from Westerly, Rhode Island, United States) for the experiments reported in this paper. The granite block was cored and polished to ring specimens. The outer diameter is 53.98 mm and the inner diameter is 44.45 mm. The rock rings were glued into the steel sample grip, and ground flat on a surface grinder to a height of 2.4 mm. The fault surfaces were then hand ground to a uniform roughness using #60 SiC powder on a glass plate. The ring specimens were jacketed both inside and outside by inner split Teflon rings and outer O-rings (Figure S2).

In the rotary shear sample geometry used in this study, the normal stress on the fault surface is a sum of the confining pressure and the axial stress. At the start of an experiment, confining pressure was raised to 20 MPa and servo-controlled within the measurement precision of 0.05 MPa. Axial load was then applied to bring the normal stress to 25 MPa. Axial load was also servo-controlled, generally to within the measurement precision of 0.07 MPa (7).

Shear displacement δ and shear stress τ are calculated from the total rotation R [*] and the torque Γ [Nm] as follows (8):

$$\delta = \frac{4\pi}{3}\frac{R}{360}\frac{r_{out}^3 - r_{in}^3}{r_{out}^2 - r_{in}^2}, \quad [1]$$

$$\Delta\tau = \frac{3}{2}\Gamma\frac{1}{\pi(r_{out}^3 - r_{in}^3)} \quad [2]$$

where r_{out} and r_{in} are outer and inner radii of the sample ring, respectively. Data were collected at a sampling rate of 50 Hz throughout the experiments.

2. Servo control resolution and resulting velocity resolution

Figure S5A shows measured shear stress and resolver displacement and inferred sample slip (from Eq. 5, main text) from a 10,000 s hold which started from steady-state sliding at a velocity of 0.03162 μms^{-1}. During the pre-hold steady state sliding the shear stress is constant, but shows some high-frequency oscillations due to electronic noise. During this time the resolver displacements increase at a constant rate (not shown on the plot due to the sensitive scale of the resolver plot). For the same reason the inferred sample displacements are also not shown during steady sliding. During the hold the resolver (load-point) displacement is servo-controlled to be constant ($V_{\rm lp} = 0$). But, as shown in Figure S5B, the resolver position undergoes abrupt variations having a magnitude of slightly less than 10 nm (these are control system corrections, arising from the finite resolution of the resolver), which is consistent with the expected 9.2 nm resolution for the resolver displacement. The measured shear stress as shown in Figure S5 helps to understand what is occurring in terms of actual fault slip and resolver load-point motion during the hold, even in the time intervals where the resolution of the resolver leads to uncertainty in the load-point motion. During the periods between the 9.2 nm "spikes" when the resolver signal is constant, the shear stress is slowly increasing (Figure S5B). Referring to equation (5) of the main text, this can only be due to forward motion of the load point or backward motion of the fault. Given that backward motion of the fault is impossible without changing the sign of the shear stress, forward motion of the load point must occur that is too small to be measured by the resolver. The reason for this forward drift of the displacement and shear stress between the servo corrections is likely that oil in the hydraulic cylinders slowly leaks past the internal piston in them due to pressure differences in the two chambers that arise from a combination of their different internal areas and the externally applied force. However, continued forward motion of the load eventually results in enough motion that it is measured by the resolver. The servo control using the resolver as feedback then corrects the load-point position, moving it back to the intended constant value. This results in a rapid decrease in the shear stress as is shown in Figure S5B. The calculated fault slip in Figure S5 assumes that during the hold the load point displacement is zero, which is correct at the scale of the hold portion of Figure S5A, and so the gradual overall decay of the shear stress and the gradual overall increase in fault slip shown there is correct. However, on the scale of Figure S5B the incorrect assumption of no

displacement of the load point between the corrective spikes, together with the observed increase in the shear stress, leads to a erroneous calculation of a decrease in fault slip between the spikes. Immediately following each servo correction, the decrease in the shear stress leads to a calculated increase in fault slip.

As the indicated slope on the plot of fault slip in Figure S5A shows, the slip velocity near the end of this specific hold gets as low as 0.02 nms^{-1}. The largest error in estimating the slip rate must accompany near instantaneous variations in the resolver position by 9.2 nm. Across such rapid resolver motions, the sample's motion at an average at 0.02 nms^{-1} can be ignored. This resolver motion would, under these circumstances, lead to a change in the shear stress of magnitude $\Delta\tau = k\sigma\delta_{1p}$. To estimate the magnitude of slip rate variations this change in shear stress could cause, which is the uncertainty in our slip rate estimation, we turn to the rate-state friction equations, which seem to do a good job describing our experiments at the lowest sliding speeds we can resolve. Assuming the load point motion to be nearly instantaneous, one can assume that this shear stress change will be balanced by the change in friction due almost entirely to the direct velocity effect. This assumption is likely accurate even for 'non-instantaneous', sub 9.2 nm, excursions in the resolver. From eq. 1 of the main text, we get

$$V = V_0 \exp\left(\frac{\Delta\tau}{a\sigma}\right) = V_0 \exp\left(\frac{k\sigma\delta_{1p}}{a\sigma}\right). \quad [3]$$

Using $k = 0.065\,\mu m^{-1}$, $\delta_{1p} = 9.2\,\text{nm}$ and $a = 0.013$, we get $V/V_0 \sim 1.05$ for positive changes in load point displacement suggesting that the actual velocity does not vary by more than 5% from the average of 0.02 nms^{-1}. Note that this estimate is independent of the long-term, background slip rate as long as the ~ 10 nm fluctuations in load-point displacement occur at orders-of-magnitude faster rates than the slip rate. Therefore, the velocity resolution in these experiments is roughly 5% near the termination of long holds.

3. Notes on the Slip and Aging equation fits to the velocity steps

The methodology used to fit the velocity step decrease data shown in the main text is described under the *Materials and Methods* section accompanying the main text. Here we present a brief discussion on the principal features of these fits. The data from the velocity step decreases shown in Figure 1 in the main text were fit with the Slip equation in two ways – a common fit to a subset of the velocity steps and independent fits to all the velocity steps. For the first of these, the initial $3\mu m$ of post-step friction evolution for one each of 1.0, 2.0, 2.5, 3.0 and 3.5 order steps were fit with a common set of Slip equation parameters. These Slip equation fits are shown in Figures S7A-E. Even though the fits to the steps are reasonable, the post-peak friction evolution is underestimated for the 3.0 and 3.5 order steps (Figure S7A and B) but overestimated for the 1 order step (Figure S7E). In particular, these patterns of misfit seem consistent with too small a value of D_c being used for the fits compared to the data from the two largest step which, at the same time, is slightly too large compared to the data from the smallest step. The value of a for these fits is around 0.013 and $D_c \sim 2\mu$m. Figures S7F-J show the slip rate evolution predicted by the corresponding fits to the friction data. All the fits capture the slip rate excursions reasonably well. It is also noteworthy that the value of $a - b$ derived from the fits is -0.0031 which is in good agreement with the independent estimate of $a - b$ in Figure S6. The Slip equation simulations in Figures 1, 2 and 3 and Table 1 in the main text use the parameters derived from these first set of fits.

To further explore the slight step-size or slip-rate dependence of D_c suggested by the fits in Figure S7, we tried a second family of Slip equation fits to the velocity steps by allowing independent fits to every velocity step decrease in Figure 1 with $a - b = -0.003$. As with the fits in Figures S7 and S8, we fit friction evolution over only the first 3 μm of post-step slip. Figure S9 shows these fits while Figure S10 the corresponding predictions of slip rate. While the data from each individual step is very well matched by the particular parameter choices for that fit, the Slip equation parameters do vary somewhat across these different fits. The most pronounced is the variation of D_c, but even that varies by a factor of less than two. These variations can be seen in the posteriors of both a and D_c in Figures S11A-D. The panels A and B in these figures show the posteriors for the 0.5 and 1.0 order steps alone, while the panels C and D show their corresponding variations for the MCMC fits to the larger steps. Comparing the posteriors of a between Figures S11A and C immediately reveal that there is no statistically significant variation in a between the different models required to fit the vastly different step sizes. Interestingly, the variations in D_c required to fit the various 0.5 order steps was also found to be similar to the variations in D_c required to fit the larger steps. When either the value corresponding to the minimum RMSE fit or the median value of D_c are extracted from these posteriors and plotted as a function of the post-step velocity (inset of Figure S11B), the observed variations in D_c turn out to be within the bootstrapped 95% confidence levels suggested by the posteriors inferred from the MCMC fits. Therefore, given the data variations between the different velocity steps of the same step size, it is difficult to conclude that the variations in D_c observed between the fits to the different sized steps necessarily reflect a trend with step size.

With the Aging equation, we have tried only the one-fit-to-all-steps strategy for the velocity step decreases in Figure S7A-E. These fits are shown in Figure S8A-E. As is to be expected from the arguments presented in the main text, the Aging equation generally does a worse job of fitting the post-minimum friction evolution than the Slip equation with no a priori constraints on $a - b$ (red curves in Figure S8A-E). With the root mean square misfit for all the velocity steps weighted equally, the joint best fit to all of the steps did the best job of fitting the medium-sized steps. In particular, for the largest slip rate decreases the fitted friction evolved to steady state over a smaller slip scale than the data. Also, these fits required $a - b = 0.0035$ which is clearly at odds with our independent estimate of $a - b = -0.003$ in Figure S6. Bhattacharya et al. (6) have shown that the Aging equation needs to be velocity strengthening in order to match the monotonically decreasing stress relaxation trajectories observed during long holds. In keeping with the view that holds are similar to the pre-minimum strength evolution

following large velocity steps (Figure 3C-F in the main text), it seems reasonable that only velocity-strengthening Aging equation solutions allow the friction minima to monotonically decrease in response to increasing step size at a rate comparable to the data. For completeness, we also present Aging equation fits to the data with the a priori constraint $a - b = -0.003$ (purple curves in Figure S8A-E). In keeping with the analytical prediction that a velocity-weakening Aging equation fit would predict much shallower friction minima compared to the data for large velocity steps (as discussed in the main text), these fits grossly under-predict the friction minima for the largest velocity steps. This shows that the failure of the Aging equation to fit the velocity step decrease data is inherently connected to its failures in fitting stress evolution during long holds (6). The Aging equation simulations in Figures 1, 2 and 3 and Table 1 in the main text use the parameters derived from these set of fits with the Aging equation.

4. Slip scale for friction evolution following large Aging-equation velocity-step decreases

One of the features of Aging equation simulations incompatible with the 'short slip distance' strengthening observed after the stress minimum in our velocity step decreases is the ever-decreasing length scale of strength evolution with increasing step size (Figure 1B in the main text). Here, we rationalize this feature for velocity decreases that push the interface far below steady state ($V\theta/D_c \ll 1$). To do this, we approximate the post-minimum friction evolution under the Aging formulation as

$$\frac{d\mu}{d\delta} \approx b\frac{d}{d\delta}\ln(\theta) \approx \frac{b}{D_c}\frac{D_c}{V\theta}, \qquad [4]$$

where δ is slip distance. The first equality in Eq. (4) follows from equation (1) with a near-constant sliding velocity (equal to V_f), and the second from the Aging law approximation $\dot{\theta} \approx 1$ far below steady state. In Figure S12, we show that for Aging-equation velocity step decreases, $V\theta/D_c$ shortly beyond the strength minimum (we choose an arbitrary level at 0.9 of the total stress drop) is only modestly larger than the velocity ratio V_f/V_i. This is because V is slightly above V_f and θ is modestly above $\theta_i = D_c/V_i$. Thus, the Aging formulation predicts that the rate of restrengthening $d\mu/d\delta$ just beyond the stress minimum increases almost as rapidly as V_i/V_f.

The above result is for a finite-stiffness system. For an instantaneous velocity step applied directly to a surface previously sliding at steady state, or equivalently a load-point velocity step in an idealized infinite-stiffness system, the Aging equation (2a) in the main text can be integrated analytically for θ and the result substituted into the friction equation (1). Relative to the future steady-state value, the friction is (9)

$$\Delta\mu = b\ln\left(1 + \frac{(V_f - V_i)e^{-\delta/D_c}}{V_i}\right) . \qquad [5]$$

Differentiating with respect to δ and evaluating at the stress minimum ($\delta = 0$),

$$\frac{d\mu}{d\delta} = \frac{b}{D_c}\left(\frac{V_i}{V_f} - 1\right). \qquad [6]$$

For large step decreases $V_i/V_f \gg 1$, $d\mu/d\delta$ increases linearly with V_i/V_f. The Tullis rotary shear apparatus is stiff enough that Aging formulation simulations that use its stiffness qualitatively capture this infinite stiffness result.

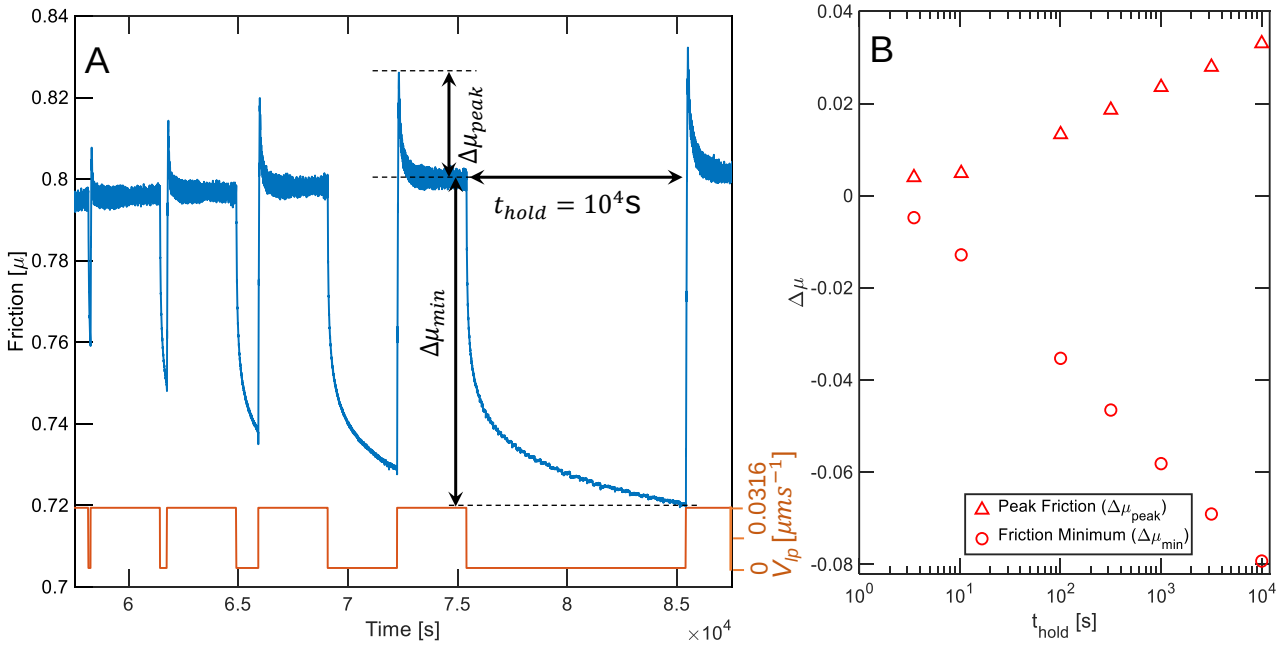

Fig. S1. Frictional strengthening in laboratory slide-hold-reslide experiments. (A) Variation in friction (blue) and loading rate (orange) with time during a sequence of slide-hold-reslides for the section of the experiments shown in Figures 4B and E. (B) Evolution of peak friction and the friction at the end of the holds with hold duration from the same experiment section. The data shows the classical linear with log hold duration increase in the peak friction. Also note the also nearly linear with log hold duration decrease in the minimum friction shown by the data. Such continual decrease in the friction minimum is generally inconsistent with a velocity weakening Aging RSF model (6).

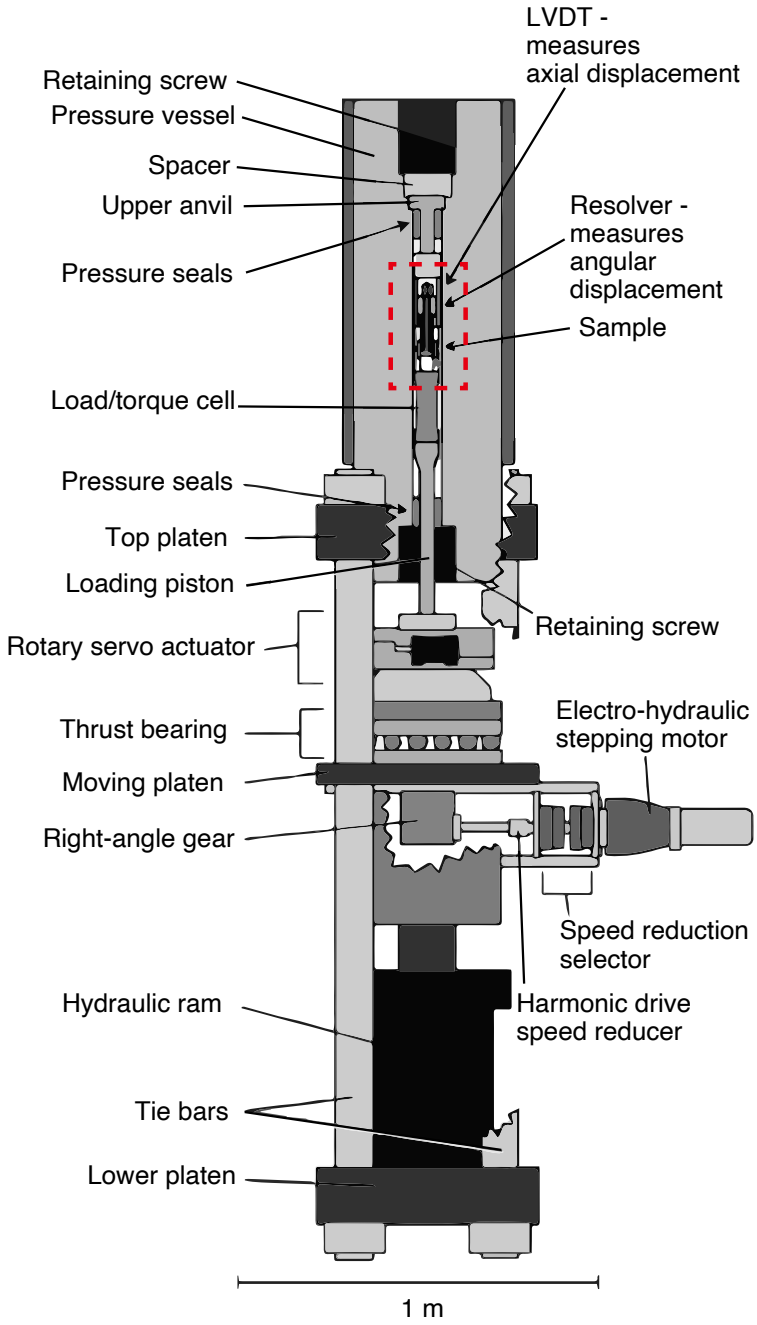

Fig. S2. Schematic of the rotary shear apparatus at Brown used for the experiments in the paper. The major parts are labeled.

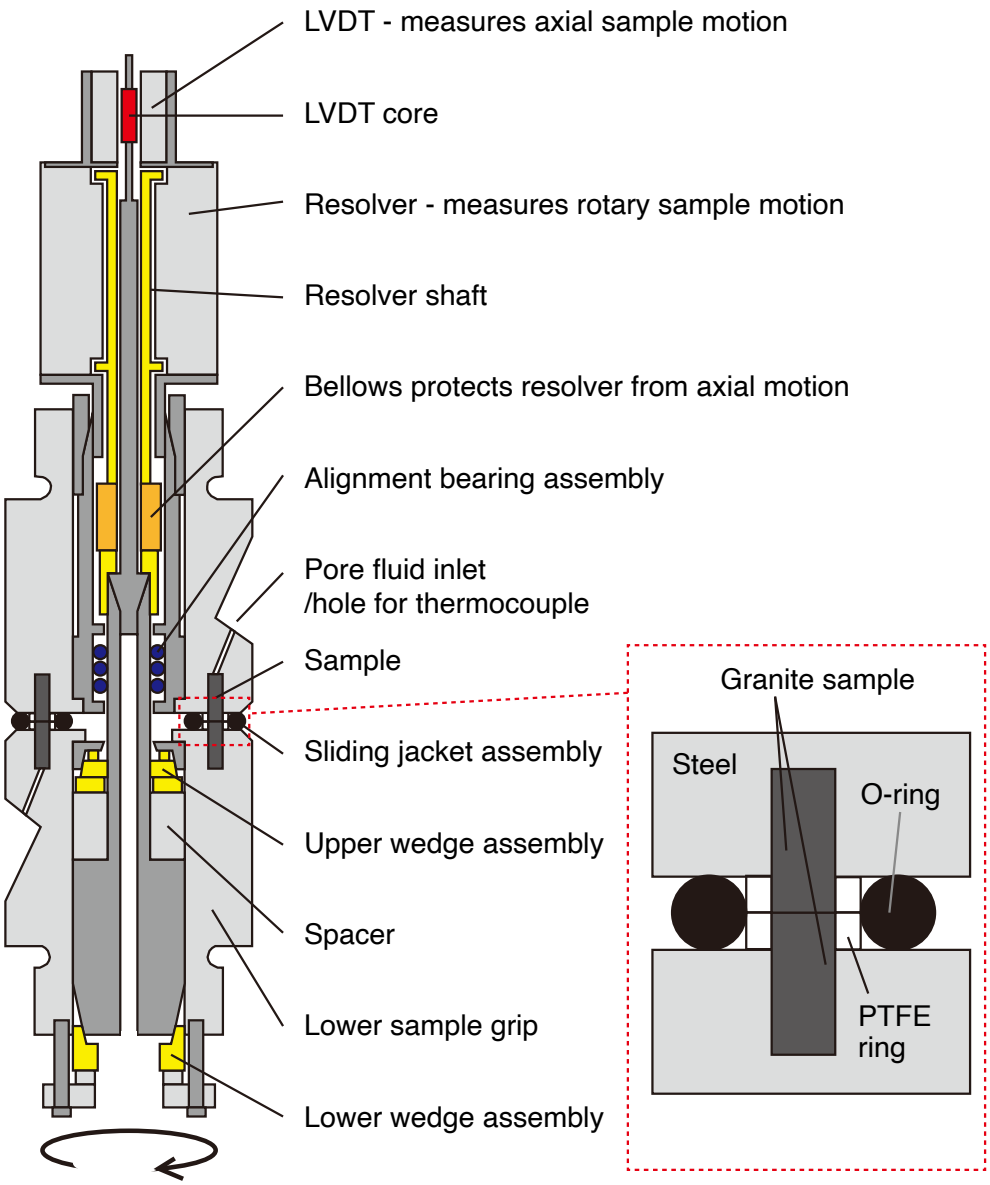

Fig. S3. Close-up view of the region enclosed by the dashed, red rectangle in Figure S2 showing the pressure vessel, sample assembly and the measurement set-up. On the right inset, the sample assembly showing the granite ring sample, the sample grips and the O-ring.

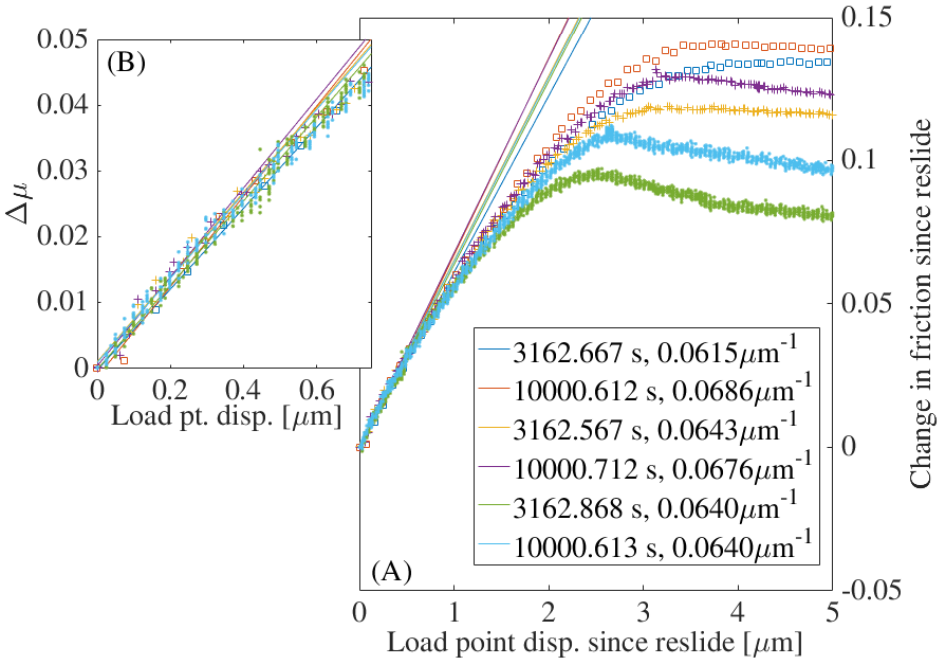

Fig. S4. Estimation of stiffness for the servo-controlled, artificially stiffened, rotary shear apparatus. (A) Change in friction ($\Delta\mu$) since reslide versus load point displacement (δ_{lp}), both evaluated since the start of the reslide, following holds of ~ 3000s and ~ 10000s at three reslide rates each – squares at 1 $\mu\mathrm{ms}^{-1}$, crosses at 0.3162 $\mu\mathrm{ms}^{-1}$ and dots at 0.03162 $\mu\mathrm{ms}^{-1}$. The initial reloading rate fixes the stiffness; we used 1/7th of the total number of points between the onset of reslide and eventual peak strength for the fits. (B) A zoomed in version of the fits in (A). We use a stiffness of 0.065 $\mu\mathrm{m}^{-1}$ in our analyses.

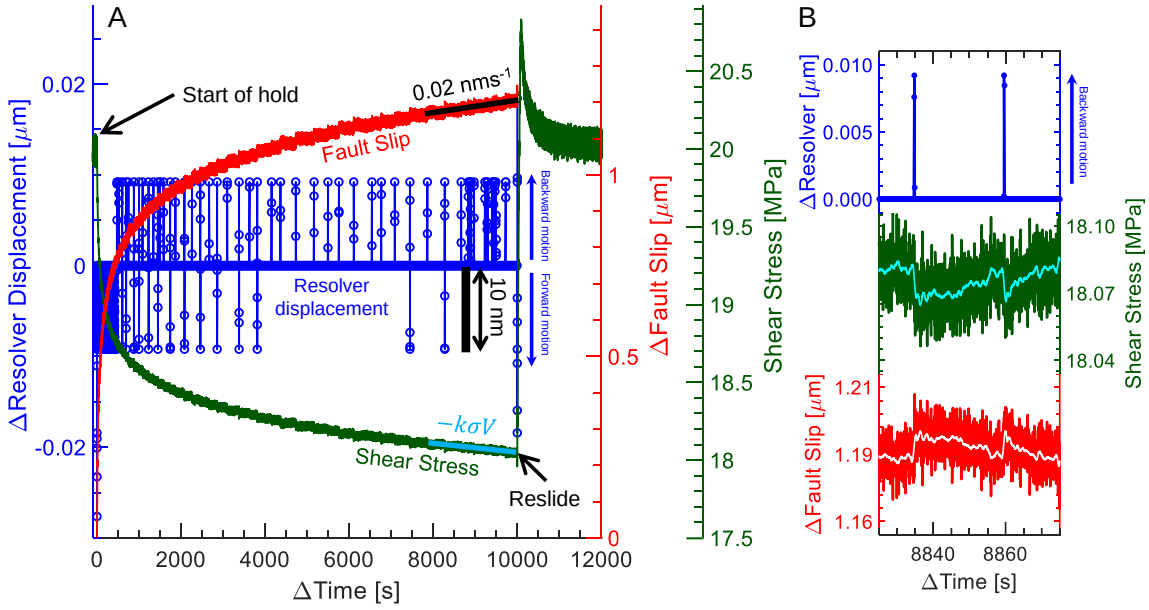

Fig. S5. (A) Shear stress, load-point displacement, and fault slip during a 10,000 s hold, following steady-state sliding at 0.0316 $\mu\mathrm{ms}^{-1}$. The load-point displacement is servo-controlled to be constant during the hold to a resolution of 10 nm, which allows attaining very small fault-slip displacements and velocities. The shear stress (green curve) is measured with a torque-cell and the load-point displacement (blue curve) is measured with a high-resolution resolver, both being mounted internal to the pressure vessel. Note that some blue data points from the resolver appear to suggest even better resolution than 10 nm, but these data points result from some temporal averaging; they reflect contributions from values at the nominal one as well as from values differing by 10 nm. Averaged over time windows encompassing many resolver "corrections", small changes in shear stress result from relaxation of the frictional stress due to slowing fault slip. This fault slip can be calculated (red curve) using the known stiffness of the rock between the fault and the load-point and knowledge of the load-point displacement. As shown by the slope of the red curve near the end of the hold, the average fault slip velocity becomes as low as 0.02 nms^{-1}. The corresponding rate of decrease in shear stress, $k\sigma V$ with $V = 0.02\mathrm{nms}^{-1}$, is also shown to capture the trend in the shear stress data very closely. As discussed in the text, the variations in this average velocity are estimated to be only 5 percent due to the 10 nm displacement corrections at the load-point resulting from the servo control resolution. (B) Zoomed in view of the transient shear stress changes in response to the resolved fluctuations in the resolver position between 8825 and 8875 seconds. Note how rapid stress decreases always accompany resolvable backward movements of the load point. Also note the subsequent slower increase in shear stress even when the load point shows no resolvable motion. This can only happen when the resolver moves forward by less than 9.2 microns even though the data shows it to be nominally at rest.

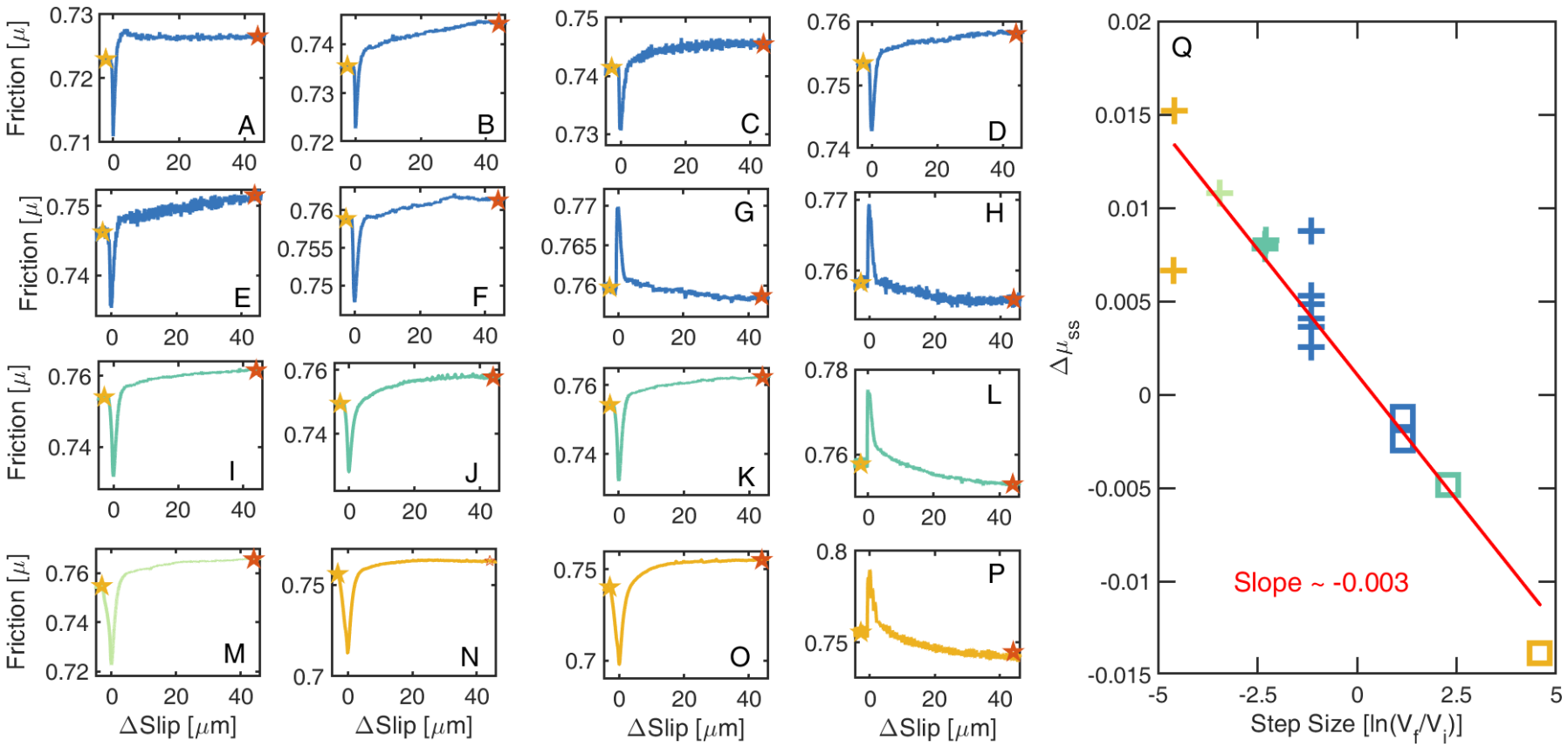

Fig. S6. Estimation of $a - b$ from all the 0.5 to 2.0 order velocity steps in Figure 1. (A)-(P) Velocity step increases and decreases of 0.5 to 2.0 orders showing steady state velocity weakening beyond total accumulated slip of 120 mm (16 in total) since the beginning of the experimental run. Color coding of the data according to step sizes is identical to the one used in the figures in the main text. The steady state change in friction, $\Delta\mu_{ss}$, is measured between the points shown by yellow and red stars in each panel. In particular, the post-step steady state is assumed at 40 μm of slip since the onset of the step to avoid long-term transients in the data. For most of the larger velocity steps excluded from this analysis, measurements had either not been continued for long enough to reach steady state or the shear stress did not saturate to a steady state level consistent with the vast majority of other velocity steps. (Q) $\Delta\mu_{\rm ss}$ versus $\ln(V_{\rm f}/V_{\rm i})$ from the sequence of velocity steps shown in (A)-(P). Mean $a - b \sim -0.003$ explains the data well.

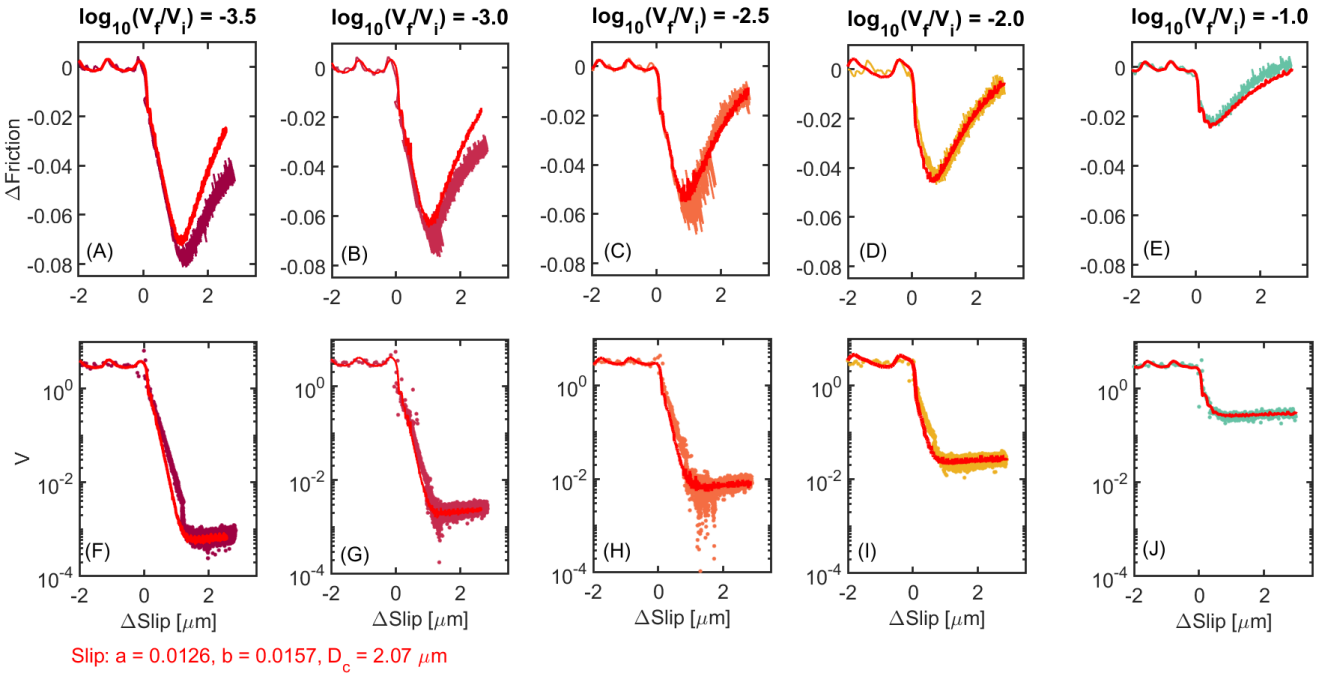

Fig. S7. Fits to a subset of the sequence of large velocity step decreases from Fig. 1A with the Slip equation jointly with the same set of parameters. Friction evolution was modeled for only the first 3 μm of slip following the onset of the velocity step to avoid potential problems with the long-term stress transients seen in some of the steps. (A)-(E) Fits to the stress data, (F)-(J) predictions of slip rate from the corresponding fits to the stress data. The data is color coded identically to the figures in the main text, Slip equation fits are shown in red. Note that $a - b$ was not pre-constrained; the inversion constrained a value which agrees well with our independent, a priori estimate of $a - b$.

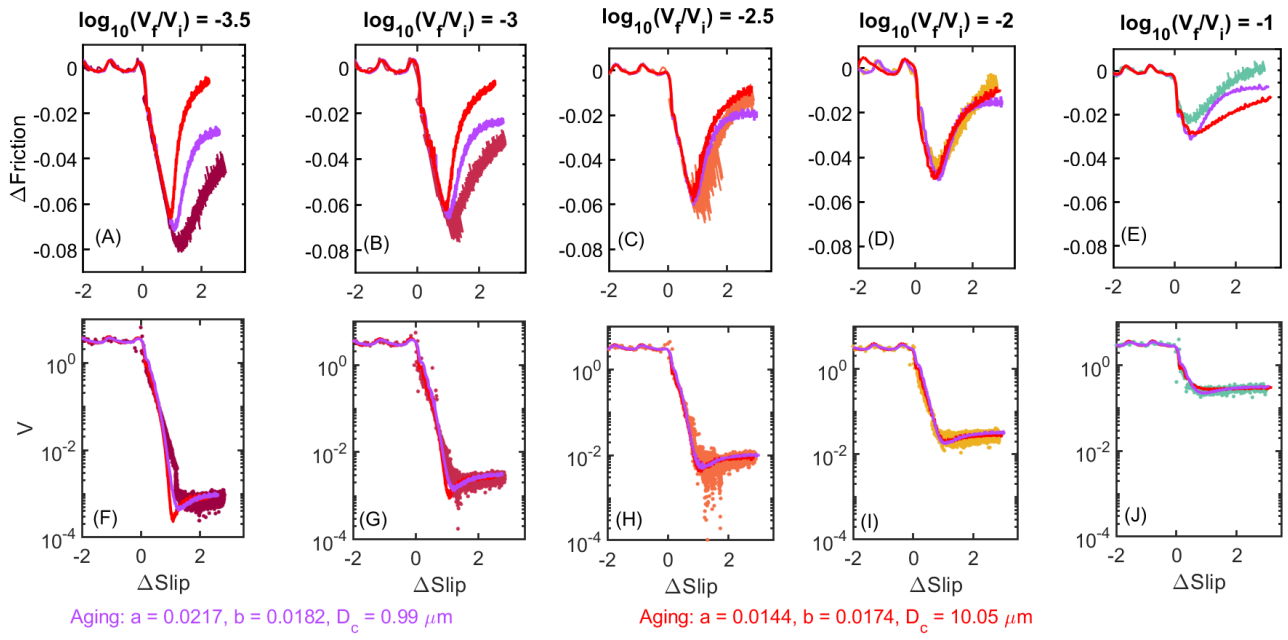

Fig. S8. Aging equation fits, with equivalent weights, to the same sequence of velocity steps in Fig. S7. (A)-(E) Fits to the stress data, (F)-(J) predictions of slip rate from the corresponding fits to the stress data. The data are once again color coded identically to the figures in the main text and Figure S7. The Aging equation fits in red were constrained with $a - b = -0.003$. Aging equation fits with $a - b$ unconstrained are shown in purple. Note that the fits with $a - b$ unconstrained naturally require $a > b$, unlike the corresponding Slip equation fits.

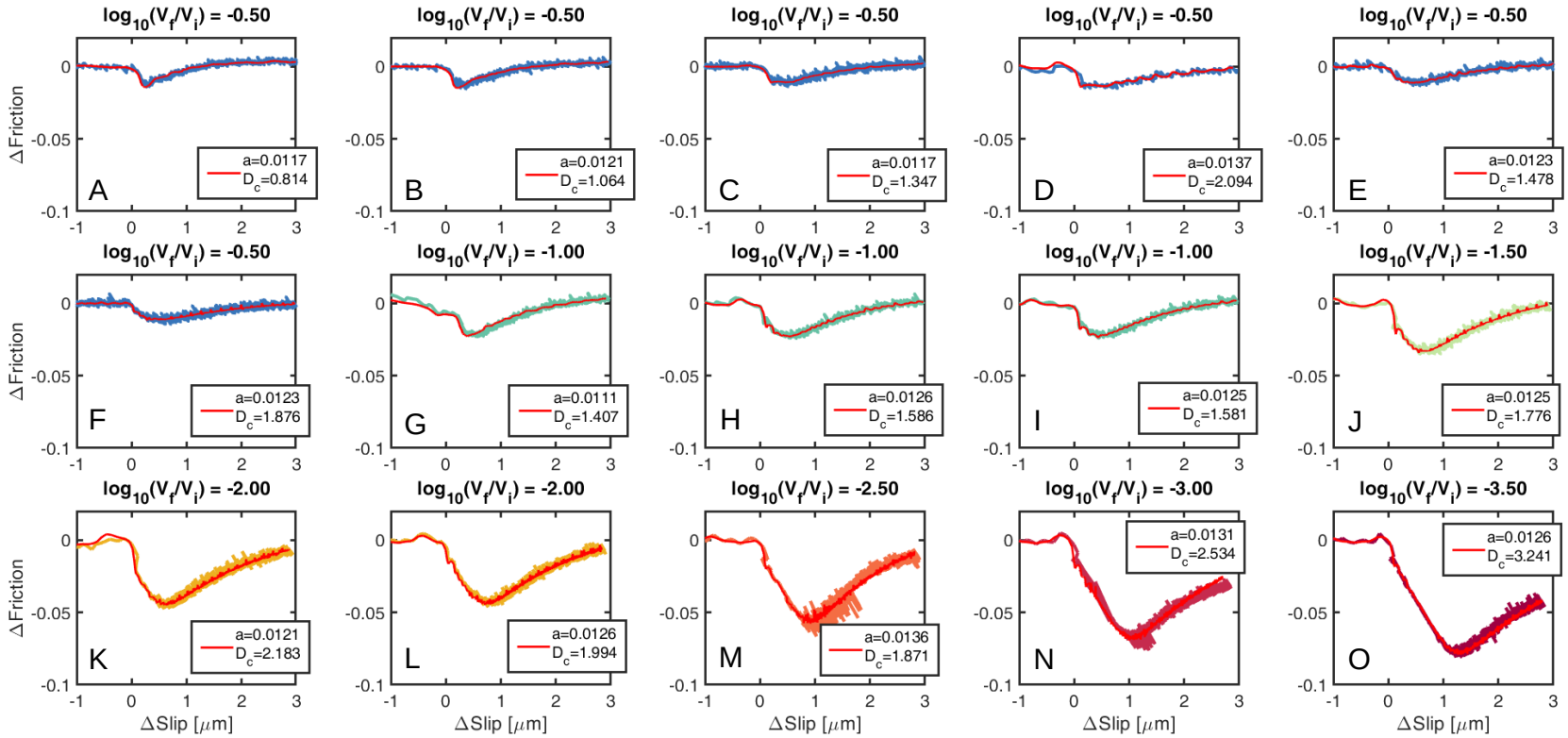

Fig. S9. Independent Slip equation fits to each of the velocity step decreases in Figure 1 from the main text. The different parameters for each of these fits are shown in the legend in each panel. Each of these fits was constrained with $a - b = -0.003$. The data are color coded according to step size identically to Figures 1, 2 and 3 in the main text. The red curves show the modeled friction response.

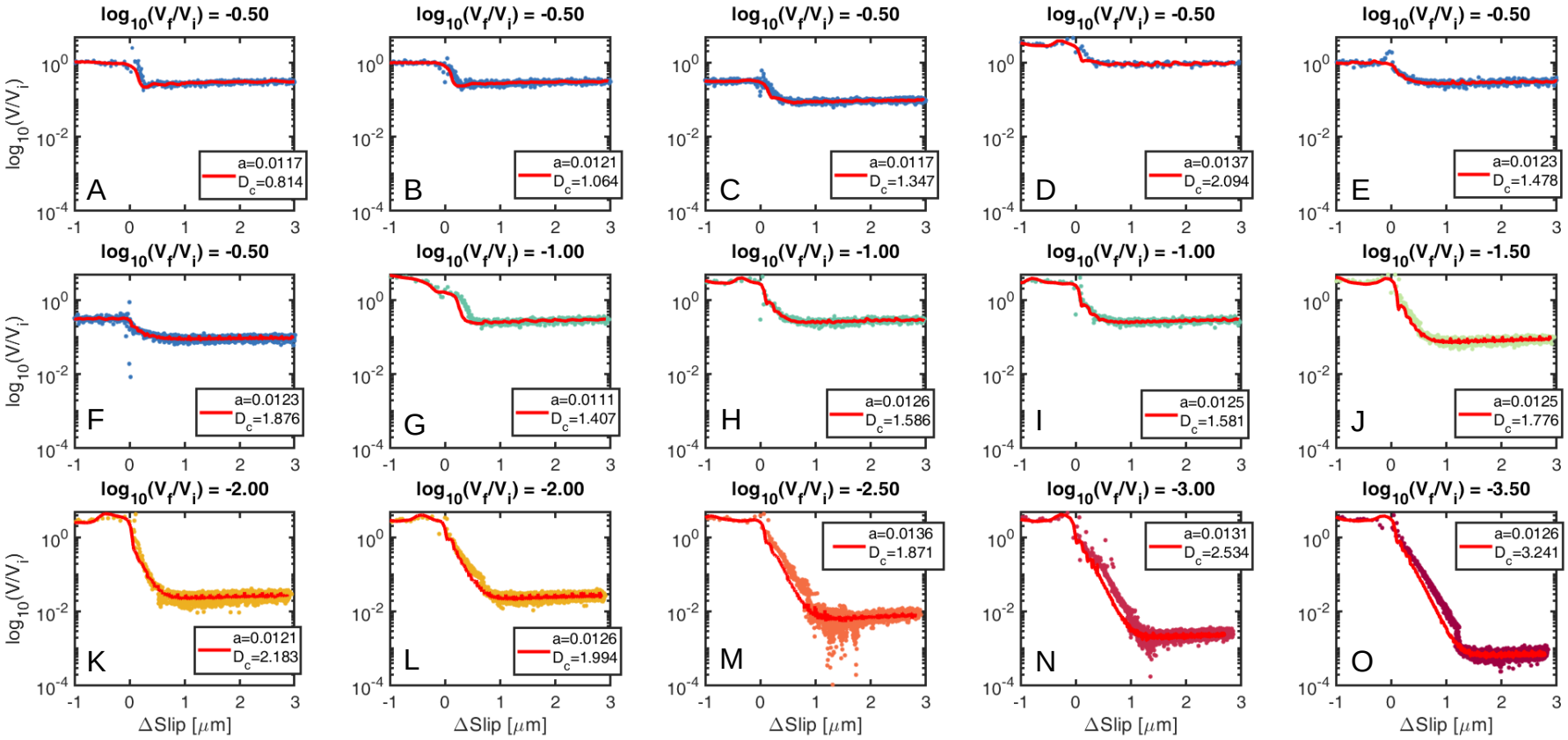

Fig. S10. Velocity predictions from the Slip equation fits in Figure S9 compared to estimated velocity variations from the data. Once again, the data are color coded according to step size identically to Figures S9. Red curves show slip rate variations estimated from the modeled fits in Figure S9.

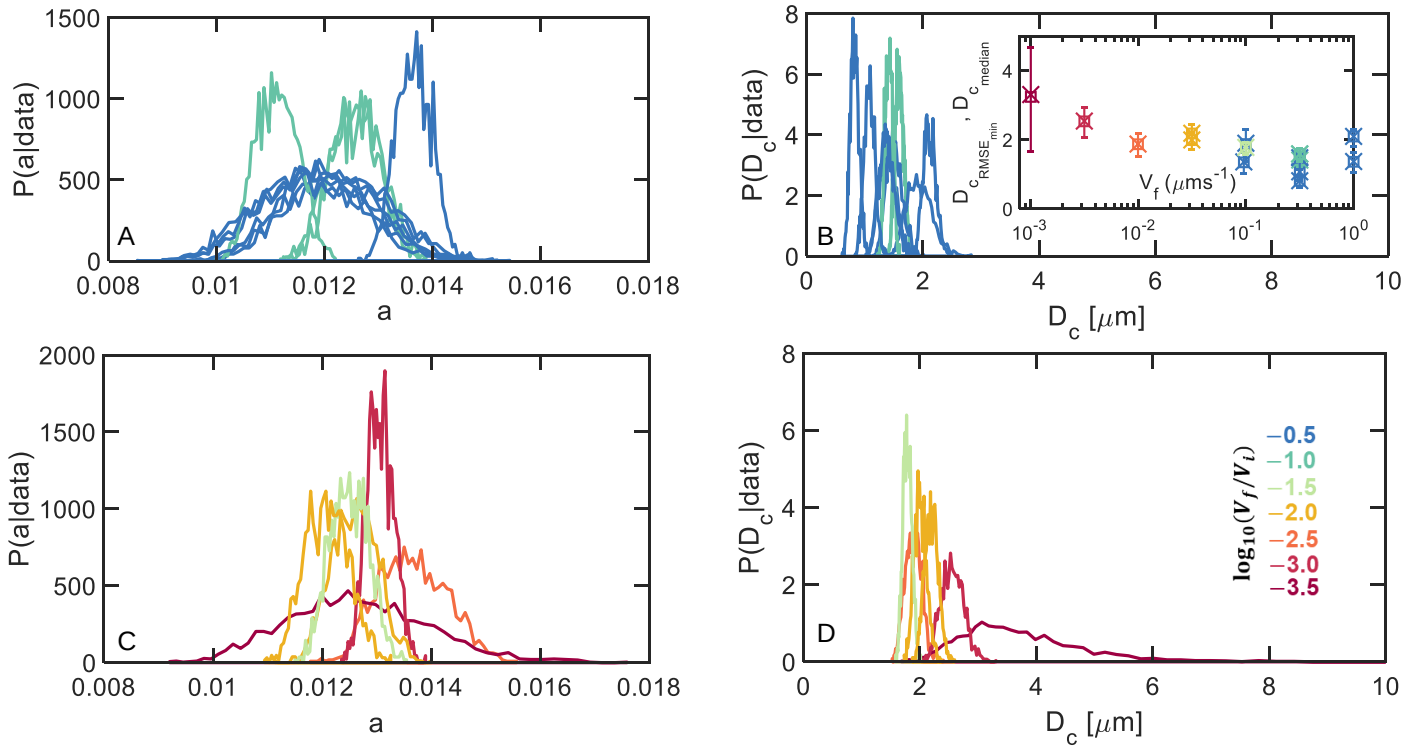

Fig. S11. Posteriors for a and D_c from the Slip law fits in Figure S9. (A) and (B) show the posteriors for 0.5 and 1 order steps, (C) and (D) for the larger step decreases. The posteriors are color coded according to step size identically to Figures 1, 2 and 3 in the main text. Inset of (B) - D_c estimates from the minimum RMSE error parameter combination found from sampling the posterior (squares) and the medians from the posteriors (crosses with 95% error bars).

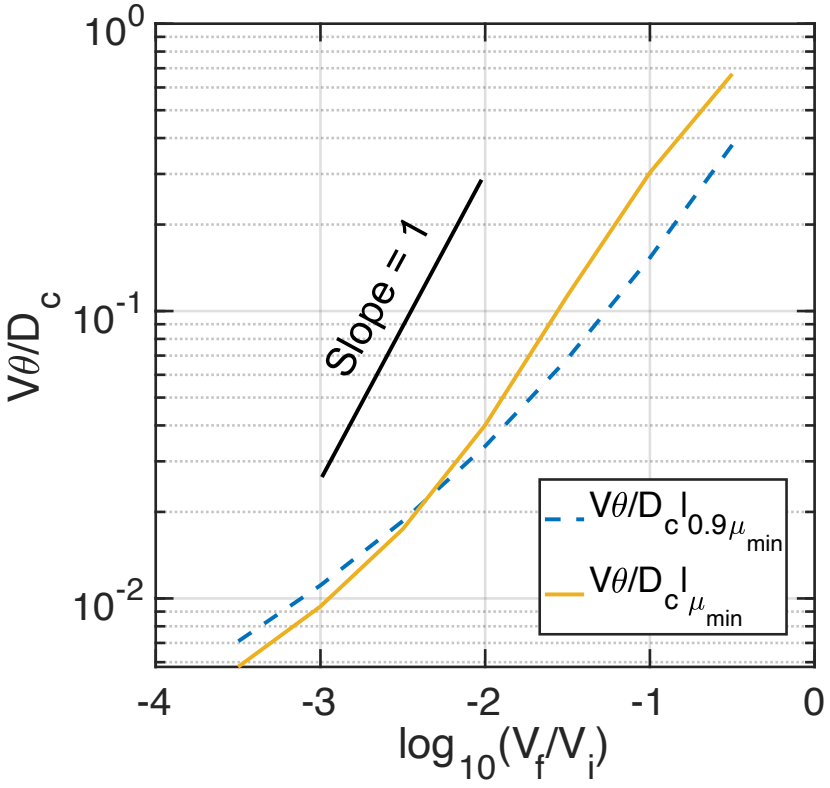

Fig. S12. Evolution of the value of $V\theta/D_c$ evaluated at strength minimum $\mu_{\min}$ (yellow solid line) and at $0.9\mu_{\min}$ post-minimum (blue dashed line) with size of velocity step decreases for the Aging equation. Model parameters were derived by fitting the velocity-step decreases in Figure S8 with the Aging equation (Table 1). Note that $V\theta/D_c$ at $\mu_{\min}$ (and also at $0.9\mu_{\min}$ post-minimum) decreases sub-linearly with increasing step size.

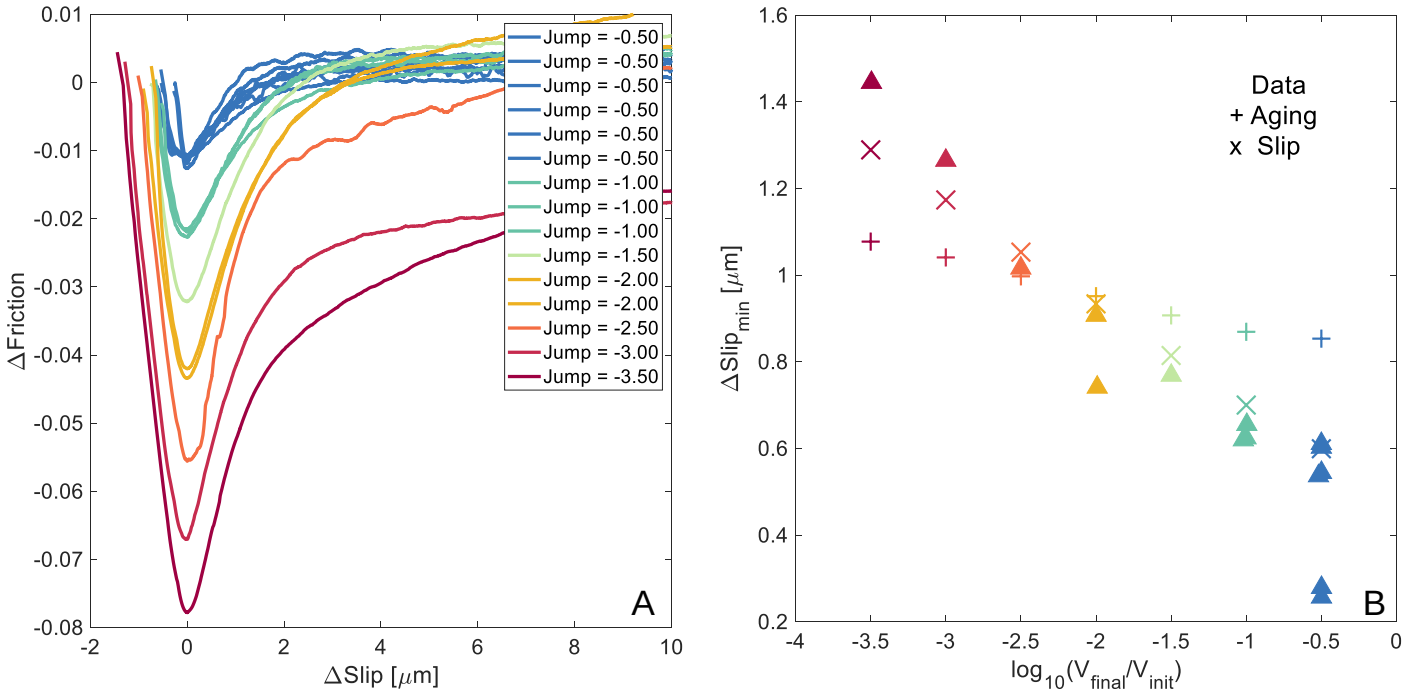

Fig. S13. Estimation of the slip accrued between the onset of the velocity step decreases in Figure 2A and the stress-minima – (A) The velocity-step data is shown again for comparison; (B) Comparison between the pre-minimum slip distance from the data (triangles), Aging equation simulations from Figure 3A (+ signs) and Slip equation simulations from Figure 3B (x signs). The color of the symbol correspond to the color coding of velocity-step size in A. Note how only the Slip equation simulations agree well with the data. The Aging equation simulations also show a quasi-linear increase in the pre-minimum slip accumulation with log step size but its rate of increase is several times smaller than that of the data.

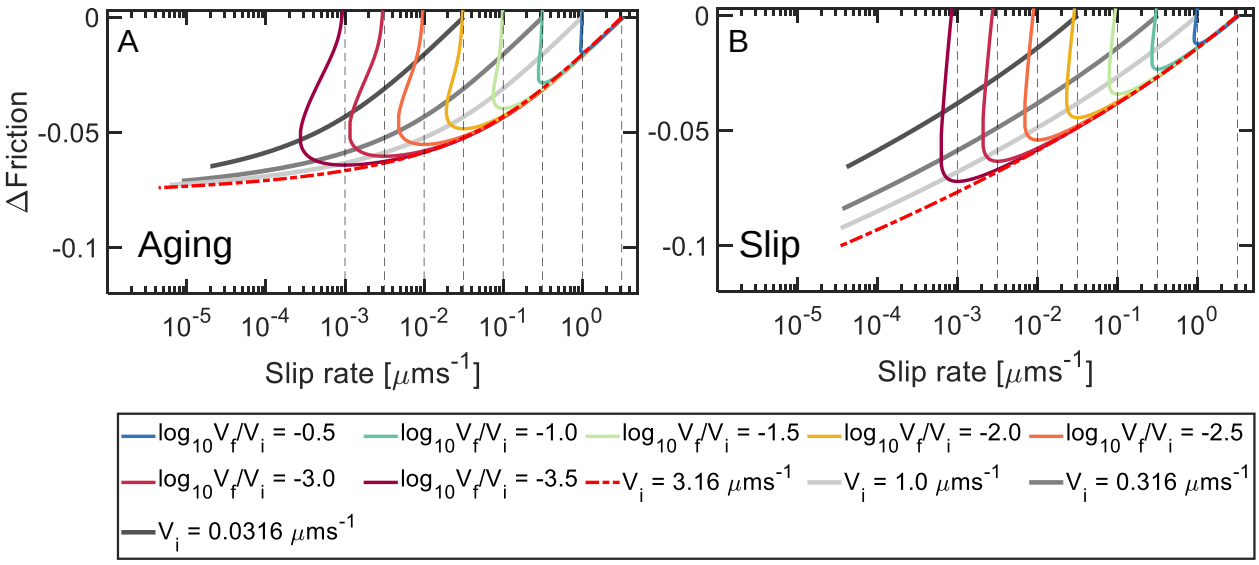

Fig. S14. Comparison of slip rate evolution during the different steps and 3163s long holds from the same set of numerical simulations shown in Figures 3(A) and (B) in the main text with the same color code. As in Figures 3(A) and (B), here (A) shows Aging and (B) Slip equation simulations. Note that the minimum velocity attained during Slip equation holds is nearly independent of the pre-hold slip rate. For the Aging equation, holds of equal duration attain smaller minimum slip rates if the initial slip rate is higher.

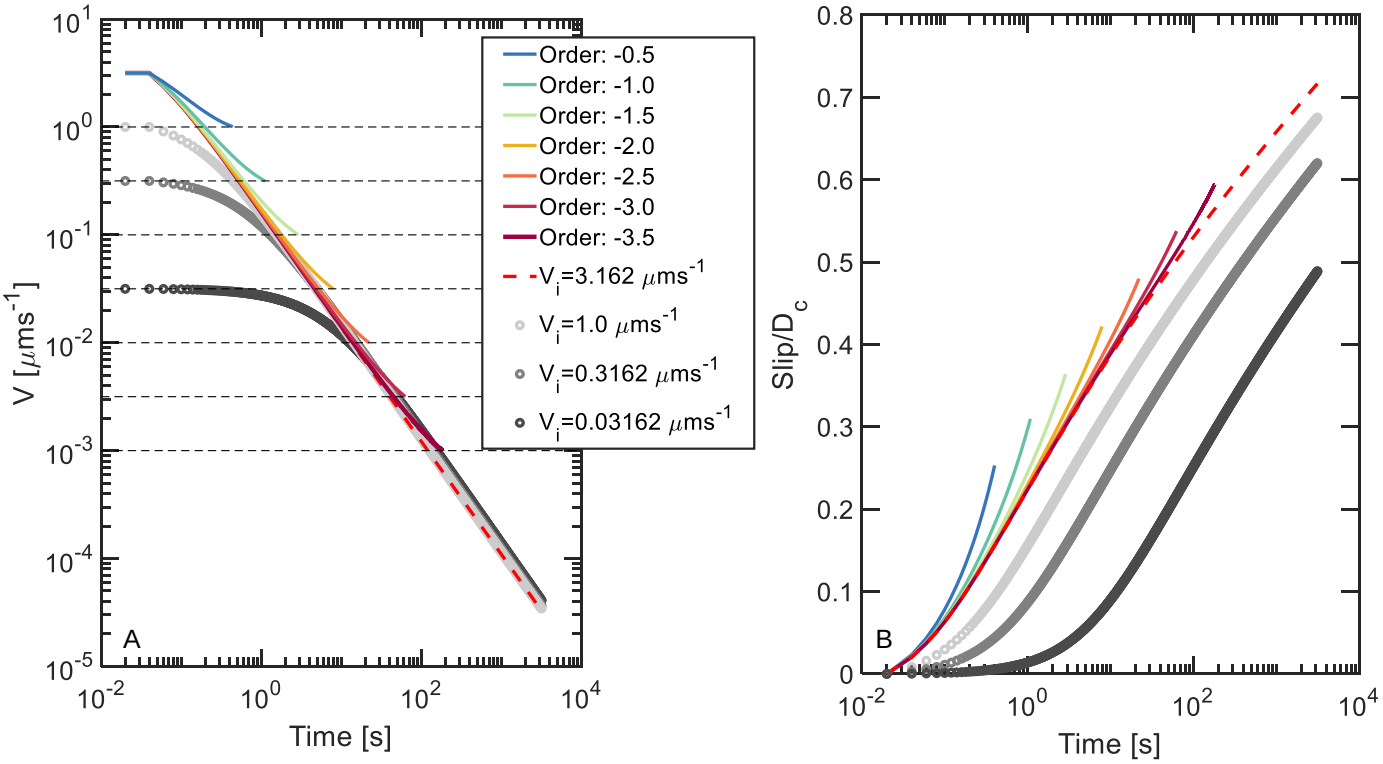

Fig. S15. Simulations of velocity steps and holds with the Slip equation parameters derived from fits to the velocity step data from Figure S7 (Table 1 in the main text). (A) Variation in slip rate with time during the pre-minimum friction evolution for the velocity steps and holds shown in Figure 3C. Note that the largest velocity steps in the experimental suite of our study access the same slip rates as hold durations of several 100s of seconds. The color scheme is identical to Figure 3. (B) Normalized slip accumulated with time for the same set of simulations as in (A). Note that the different pre-hold slip rates lead to different amounts of slip during the hold.

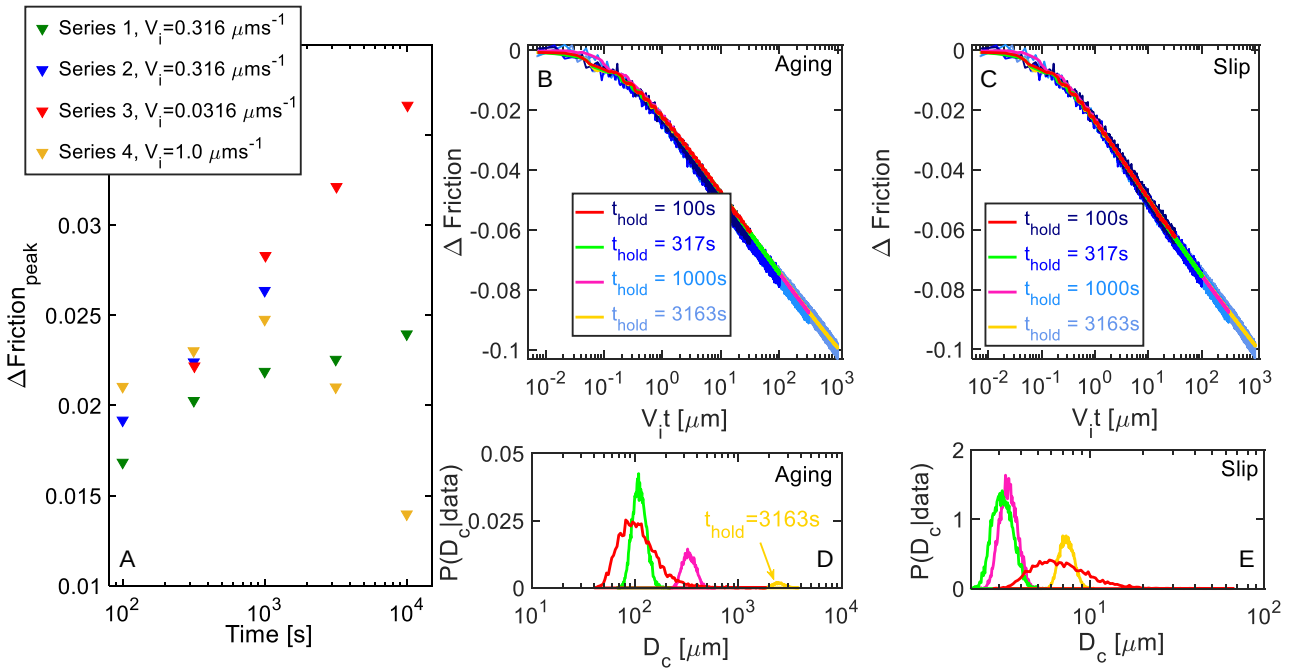

Fig. S16. (A) Peak strength evolution with hold time for all the sets of slide-hold-slides run during our experimental suite. Note the anomalous decrease in peak strength for hold durations longer than 1000 s for the set of holds with $V_i = 1\mu\text{ms}^{-1}$. This is an additional reason we chose not to fit the two longest holds at $V_i = 1\mu\text{ms}^{-1}$. (B) Aging equation joint fits to 100s – 3163s-long holds with $V_i = 0.316\mu\text{ms}^{-1}$ (Series 1 in A, not included in the main text). The 10000s hold is not included due to the MCMC not converging for this hold duration. Note that Series 2 in A is used in Figures 4A and D in the main text as representative data for $V_i = 0.316\mu\text{ms}^{-1}$. We made this choice since those data closely reproduced the hold-duration dependence of peak strength for the other sets of holds at different V_i. (C) Same as (B) but for the Slip equation. The inferred parameters from these joint fits are listed in Table 1. (D) and (E) show posteriors for D_c when the holds in panels (B) and (C) are fit individually with a different a and D_c inferred from each hold, with $a - b = -0.003$ fixed. Note that the trend of inferring larger D_c for longer hold durations with the Aging law is seen here as well, though obscured slightly by the anomalous posterior for the 100s hold with both the Aging and Slip equations.

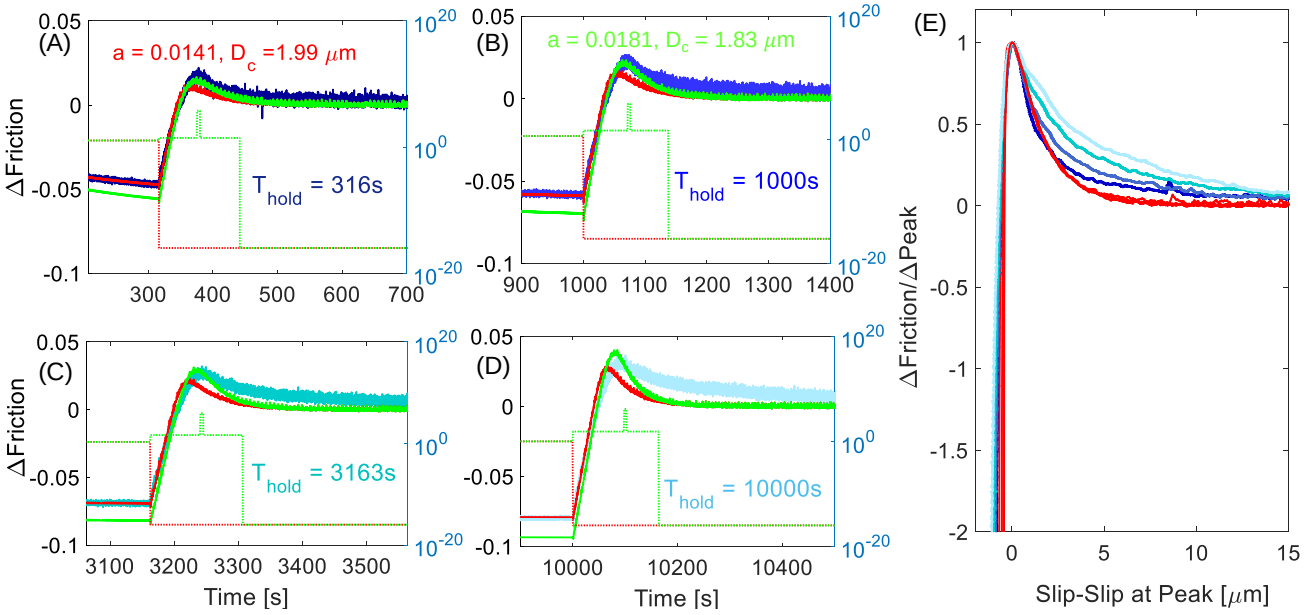

Fig. S17. Slip equation fits and predictions of the static friction peaks and evolution length scales following reslides for the set of holds in Figure 4E. (A)-(D) show the reslides following holds of duration 316 sec - 10000 sec with longer holds plotted respectively in progressively lighter shades of blue. Zero friction level is fixed at the pre-hold steady-state value of the friction coefficient. The red curves in each panel are the predictions of the fits to the holds alone taken from Figures 4E, the corresponding weights used are depicted as red dotted lines (weighting scales indicated on right axis). The green curves in each panel show fits which have been weighted equally between the hold and a fixed time window covering the reslide from its beginning to future steady state (green dotted lines). Differential weighting is applied around the peak friction to achieve maximum fidelity to the observed peak strength. Note how, when compared to the fits to the holds alone, the green curves underestimate the shear strength at the end of the preceding holds. (E) shows the strength evolution following the reslides in (A)-(D) but normalized by the peak to residual strength drop measured at 15 μm of post-peak slip. Also shown are the corresponding predictions of the fits to the holds alone scaled identically to the data (red curves). The darker to lighter shades of blue correspond to increasing hold durations as in (A)-(D). The slip weakening length scale appears to increase with hold duration.

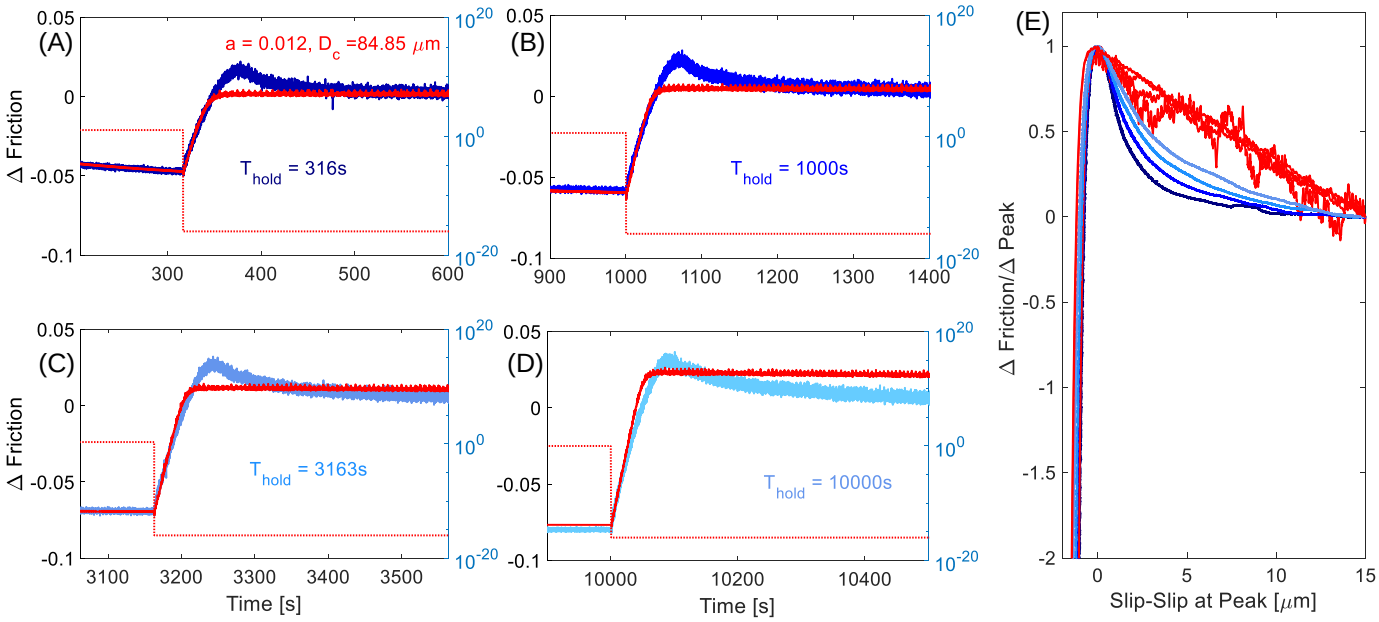

Fig. S18. Aging equation predictions of the static friction peaks and evolution length scales following reslides for the set of holds in Figure 4E. (A)-(D) show the reslides following holds of duration 316 sec - 10000 sec with longer holds plotted respectively in progressively lighter shades of blue. Zero friction level is fixed at the pre-hold steady-state value of the friction coefficient. The red curves in each panel are the predictions of the fits to the holds alone taken from Figures 4E, the corresponding weights used are depicted as red dotted lines (weighting scales indicated on right axis). (E) shows the strength evolution following the reslides in (A)-(D) but normalized by the peak to residual strength drop measured at 15 μm of post-peak slip. Also shown are the corresponding predictions of the fits to the holds alone scaled identically to the data (red curves). The darker to lighter shades of blue correspond to increasing hold durations as in (A)-(D). The Aging equation predicts strictly linear slip-weakening post-peak friction similar to its prediction for large velocity steps.

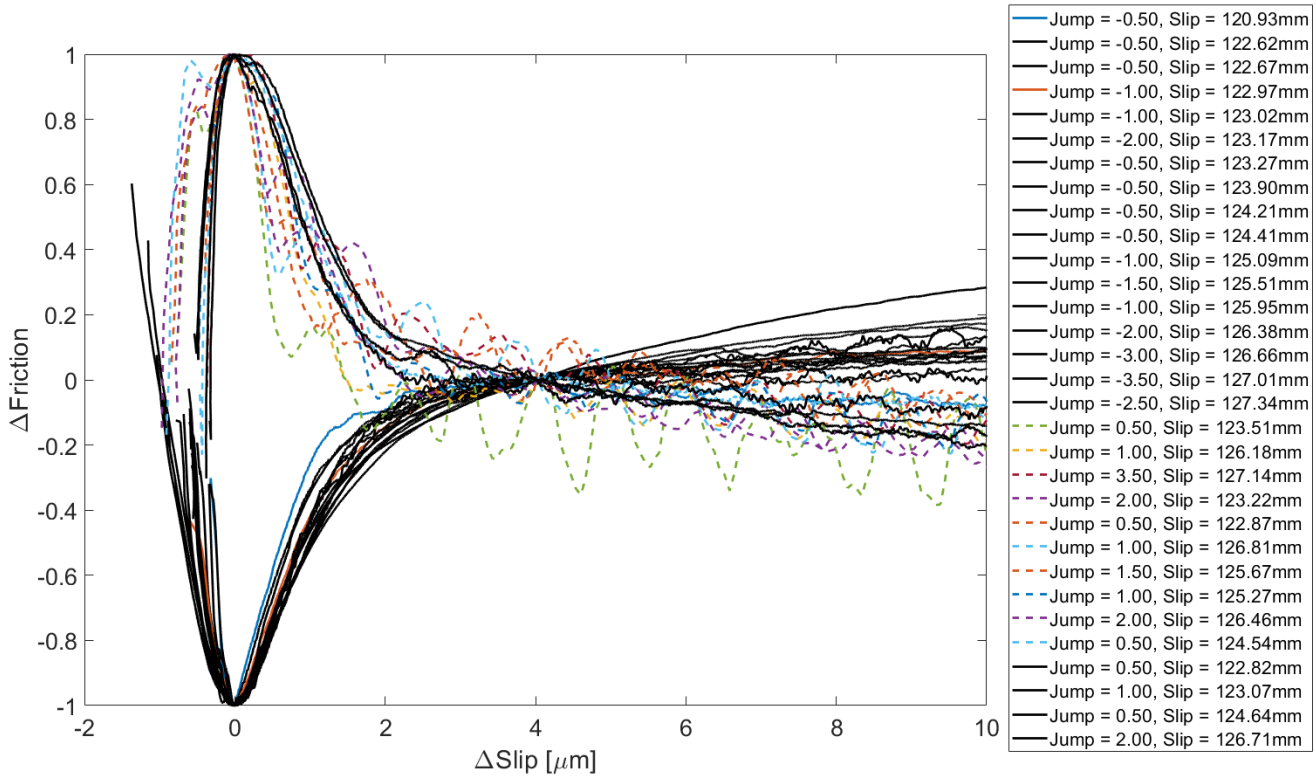

Fig. S19. All the velocity steps in the experimental run from which the ones reported in Figure 1A were chosen. As in Figure 1A, the changes in friction are measured from its value at $4\mu\mathrm{m}$ and are normalized by the maximum amplitude of this change. All the velocity steps shown in Figure 1A are shown in black. Most of the step increases were difficult to control, owing to the velocity-weakening nature of the sliding surface.

References

1. Weeks JD, Tullis TE (1985) Frictional sliding of dolomite: A variation in constitutive behavior. *Journal of Geophysical Research: Solid Earth* 90(B9):7821–7826.
2. Tullis TE, Weeks JD (1986) Constitutive behavior and stability of frictional sliding of granite. *Pure Appl. Geophys.* 124(3):383–414.
3. Beeler NM, Tullis TE, Blanpied ML, Weeks JD (1996) Frictional behavior of large displacement experimental faults. *J. Geophys. Res.: Solid Earth* 101(B4):8697–8715.
4. Tullis TE (1997) Friction measurement apparatus in *Instruments of Science: An Historical Encyclopedia*, eds. Bud RF, Warner DJ. (Garland, New York), pp. 249–251.
5. Beeler N, Tullis TE, Weeks JD (1994) The roles of time and displacement in the evolution effect in rock friction. *Geophys. Res. Lett.* 21:1987–1990.
6. Bhattacharya P, Rubin AM, Beeler NM (2017) Does fault strengthening in laboratory rock friction experiments really depend primarily upon time and not slip? *J. Geophys. Res.: Solid Earth* 122(8):6389–6430. 2017JB013936.
7. Beeler NM, Tullis TE (1997) The roles of time and displacement in velocity-dependent volumetric strain of fault zones. *J. Geophys. Res.: Solid Earth* 102(B10):22595–22609.
8. Tsutsumi A, Shimamoto T (1997) High-velocity frictional properties of gabbro. *Geophysical Research Letters* 24(6):699–702.
9. Ampuero JP, Rubin AM (2008) Earthquake nucleation on rate and state faults – aging and slip laws. *J. Geophys. Res.* 113:B01302.